HAL
open science

The 2000 Tottori (Japan) earthquake: triggering of the largest aftershock and constraints on Dc.

Sara Di Carli, Christophe Voisin, Fabrice Cotton, Fethi Semmane

To cite this version:

Sara Di Carli, Christophe Voisin, Fabrice Cotton, Fethi Semmane. The 2000 Tottori (Japan) earthquake: triggering of the largest aftershock and constraints on Dc.. 2008. hal-00204676

HAL Id: hal-00204676

https://hal.science/hal-00204676v1

Preprint submitted on 18 Jan 2008

HAL is a multi-disciplinary open access archive for the deposit and dissemination of scientific research documents, whether they are published or not. The documents may come from teaching and research institutions in France or abroad, or from public or private research centers.

L'archive ouverte pluridisciplinaire **HAL**, est destinée au dépôt et à la diffusion de documents scientifiques de niveau recherche, publiés ou non, émanant des établissements d'enseignement et de recherche français ou étrangers, des laboratoires publics ou privés.

The 2000 Tottori (Japan) earthquake: triggering of the largest aftershock and constraints on D_c.

By S. Di Carli, C. Voisin, F. Cotton and F. Semmane

Abstract

The goal of this study is to investigate the effect of the static and dynamic stress changes on the triggering of faults under slip-dependent friction law. We specifically focus on the 2000 Western Tottori (Japan) earthquake and on the triggering of its largest aftershock. To this end we compute the dynamic and static stress changes caused by the 2000 Western Tottori (Japan) earthquake for which a good knowledge of the rupture history and aftershock sequence exists. We compute the coseismic stress evolution caused by the mainshock fault, on the fault plane of the largest aftershock located 20 km SW of the mainshock. The static stress changes cannot explain the occurrence of the largest aftershock, located in a stress shadow whatever the friction coefficient that we use. Hence we propose that dynamic stresses have promoted the triggering of the largest aftershock. Using the discrete wavenumber and the reflectivity methods we compute the complete time-dependent coulomb failure function CFF(t). We investigate the influence of the adopted coefficient of friction μ', the depth and the location of the hypocenter on the shape of the CFF(t). Finally, using a non-linear slip dependent friction law with a stability/instability transition, we constrain the frictional properties of the largest aftershock fault plane knowing the state of stress on the fault and the time delay of 48 hours. We propose that D_c must be greater than 0.3 m.

1 Introduction

It is well established that fault interaction and seismicity triggering are driven by stress interaction. The widely used Coulomb failure criterion *(Kadinsky-Cade and Willemam 1982, Stein and Lisowsky 1983)* uses the concept of the static Coulomb failure stress ΔCFS and most clearly demonstrate the correlation between the triggering of earthquakes and the positivity of the ΔCFS. The Coulomb stress modelling performed for the 1992 Landers earthquake provides an excellent example of the effects of static stress changes and evidences the correlation between the aftershock distribution and mainshock induced static stress changes *(Stein et al., 1992; King et al., 1994)*.

However, this earthquake triggered remote seismicity *(Hill et al., 1993)* that conflicts with the simple static stress change theory. Dynamic stress changes were proposed to explain those remote aftershocks (*Kilb 2003*). The Mw 7.3 Hector Mine earthquake triggered seismicity in the rupture direction, near Salton Sea, 180 km south of the mainshock. *Gomberg et al. (2001)* have demonstrated that in this region, more than 50 events occurred in a few days, the first of them 59 s after the mainshock. Major earthquakes are now found to trigger the remote seismicity: the 1999 Hector Mine, California, earthquake *(Gomberg et al., 2001; Glowacka et al., 2002)* as we have seen; the 1999 Izmit, Turkey, earthquake *(Brodsky et al., 2000)*; the 2002 Denali, Alaska, earthquake *(Husen et al., 2004)*. *Kilb et al. (2000, 2002)* and *Gomberg et al. (2003)* have demonstrated that seismicity rate changes correlates better with the dynamic stress field than with the static stress changes. One open question is to set an upper limit on the time efficiency of dynamic triggering: one minute? One hour? One month? One year? In some cases the triggering of aftershocks begins at the waves arrival time: Salton Sea enhanced activity at the Hector Mine waves passage (*Gomberg et al., 2001*). In some other cases the triggering is delayed: the

1980 Irpinia, Italie, earthquake (*Belardinelli et al., 1999, Voisin et al., 2000*); the Little Skull Mountain (*Bodin and Gomberg 1994* and *Gomberg and Bodin 1994*) and the Hector Mine (*Kilb 2003*) earthquakes.

The 1980 Irpinia earthquake provides an interesting example of fault interaction due to spatiotemporal stress changes, because it ruptured several normal faults: three distinct subevent occurred nearly 20 s from each other. This delayed triggering can be interpreted in terms of frictional properties of the faults *(Belardinelli et al., 1999)*. *Voisin et al., (2000)* have investigated the relative weight of static and dynamic stress changes in the triggering of the 1980 Irpinia earthquake sequence. They showed that for such a short delay (20s), the dynamic stress field is more important than the static stress field. Could other events associated with longer duration be explained in the same way? *Bodin and Gomberg (1994)* and *Gomberg and Bodin (1994)* have studied the triggering of Mw 5.4 Little Skull Mountain 22 hours after the Landers mainshock. They related the occurrence of this large remote aftershock to the dynamic strain tensor. *Kilb (2003)* has pointed out the correlation of the Landers, California, aftershocks map and considered the complete temporal dependence of the Coulomb stress changes. It was observed that the peak of the dynamic Coulomb function CFF(t) better correlates with the map of seismicity rate change than the static field does. This would also imply that the dynamic stress influence aftershock triggering even for long time delay (months to year) and over large distances.

Remotely triggered seismicity, related to dynamic stress changes, is in contrast with the static stress theory. Dynamic triggering may also play a major role at short distances, as suggested recently (*Kilb et al. 2000, Voisin et al. 2000, Hough 2005*). In the near field static and dynamic stress changes both range in the same order of magnitude. None of them can be neglected a priori. This suggests that they should be considered as one and only one perturbation,

in a complete Coulomb Failure Function (*Kilb et al., 2000*).

Voisin et al. (2004) studied the effect of the complete Coulomb Failure Function (CFF) on the triggering of faults under a slip dependent friction law. They have considered idealized complete Coulomb failure functions of three types. Since the static stress field at remote distance is negligible, the far field CFF is represented by a simple sine wave. In the near field they considered two CFFs: one for stress triggers, formed by a dynamic pulse followed by a positive static stress field, and one for stress shadows, formed by a dynamic pulse followed by a negative static stress field. They demonstrated the possibility of the triggering of seismicity by a dynamic stress pulse in a stress shadow zone. Stress shadows occur when an earthquake has reduced the Coulomb failure stress on appropriately oriented nearby faults. They are associated with a seismicity rate decrease *(Stein 1999)*. So the triggering of an antishock, that is an earthquake in a stress shadow is possible only if we consider a complete CFF, with the dynamic and static stress field. Triggering of aftershocks in the stress shadows is one way to prove the role of dynamic stresses. The 2000 Western Tottori earthquake provides a unique opportunity to study the stress initiation between the main rupture and the aftershocks.

The 2000 Western Tottori earthquake sequence was well recorded by the Japanese seismic networks. Moreover, the numerous aftershocks have been relocated by *Fukuyama et al., (2003)*. The seismograms as well as geodetic data were inverted to constrain the seismic rupture process and the final slip distribution (*Iwata and Sekiguchi, 2002; Dalguer et al., 2002; Peyrat and Olsen 2004; Semmane et al., 2004*). From these results, we could compute the complete Coulomb Failure Function for the 2000 Tottori, Japan, earthquake.

In the first part of this paper we will compute the static perturbation due to the rupture and test it against the aftershock locations. We will show that the largest aftershock (M 5.1) occured in a stress shadow zone. The static stress

changes cannot explain the occurrence of this aftershock.

The other possible hypothesis that we investigate is that this largest aftershock was triggered by the dynamic stress waves emitted by the mainshock. We compute the complete stress perturbation for a set of points distributed on the fault plane of the aftershock. Whatever the friction coefficient or the depth considered, the complete CFF is described by a large dynamic stress pulse followed by a negative static stress field. The dynamic computations are therefore totally consistent with the static ones. Such a dynamic pulse is large enough (both in frequency and amplitude) to trigger seismicity.

Finally, these stress perturbations are used to constrain the fault friction properties, namely D_c, of the largest aftershock. Estimates of D_c are usually provided for large ruptures like for the 1992 Landers earthquake (*Pulido and Irikura 2000*); for the 1995 Kobe earthquake (*Mikumo et al., 2003*); for the 2000 Tottori earthquake (*Mikumo et al., 2003*). These estimates are obtained either by using the peak-slip velocity of the closest seismogram (*Mikumo et al., 2003; Fukuyama et al., 2003*) or by using kinematic inversions (*Tinti et al., 2004*). We propose a different approach to estimate D_c on intermediate-scale fault planes associated to the aftershocks. We follow a three-step methodology:
1) We compute the complete CFF at the hypocentral area of the aftershock.
2) The fault length is set accordingly with the spatial content of the secondary aftershocks and the scaling law from *Wells and Coppersmith (1994)*.
3) Assuming that the fault plane of the aftershock was close to failure, we constrain D_c using the observed triggered delay. The fault geometry is derived from the sequence of secondary aftershocks associated to the triggering of the M 5.1 event. Using the empirical law derived by *Wells and Coppersmith (1994)*, we fix the fault length to 10 km. The time delay is known and is about 48 hours. Finally the state of stress on the fault is assumed to be very close to the fault strength. Because we use a finite difference code, the time delay of 48 hours is

unreachable. The methodology used in *Voisin et al. 2000* for a time delay of 20s cannot be used in the present study. However, it is possible to rule out all values of the frictional properties that lead to a fast triggering. We are able to propose that D_c of the largest aftershock fault plane must be greater than 0.3 m.

2 Static stress changes after the 2000 Tottori earthquake

2.1 Description of the 2000 Tottori earthquake mainshock and of its largest aftershock

On 6 October 2000 at 13:30 UTC, the Western Tottori Earthquake (Mw 6.6-6.8) occurred on a left-lateral strike-slip fault in the western Honshu, Japan, where very few large earthquakes have occurred since the 1943 Tottori earthquake of M 7.2 *(Kanamori, 1972)*. Our choice of the Tottori earthquake is primarily justifies by a high-resolution strong motion records (K-net and KiK-net networks operated by the National Institute for Earth Sciences and Disaster Prevention (NIED)), and a good knowledge of its slip history suggested from kinematic inversion studies *(Semmane et al., 2004)* and a good aftershocks sequence *(Fukuyama et al., 2003)*. Within the 15 years before the 2000 western Tottori earthquake, background seismicity covered the whole aftershock region of the 2000 western Tottori earthquake and several M 5 earthquakes were observed on the mainshock fault of the 2000 western Tottori earthquake (southern part of the aftershock region). *Shibutani et al. (2002)* showed that in the southern part of the aftershock region of the western Tottori earthquake, a fault existed before the mainshock, but in the northern part there was no information about the geometry of the fault. Moreover, *Yagi and Kikuchi (2000)* and *Iwata and Sekiguchi (2001)* analyzed the rupture process of the 2000 western Tottori earthquake and they found that slip occurred only in the southern part of the

aftershock region. *Sagiya et al. (2002)* reported from the analysis of Global Position System (GPS) data that the postseismic slip occurred in the northern part of the aftershock region where little slip occurred during the mainshock. The epicenter of the mainshock is located at 35.269 N and 133.357 E at a depth of 14-15 km *(Iwata and Sekiguchi, 2002)*. Within 15 min of the mainshock, the aftershocks concentrate along the southern part, where the slip during the mainshock is estimated to have occurred. By 60 min after the mainshock activity appears throughout the entire extent of the aftershock region. As time progresses, activity fills in the fault structures (Figure 1).

On 8 October at 13:17 the largest aftershock (Mw 5.1) occurred at a depth of 5250 m, about 20 km west of the mainshock area. Its fault mechanism is left lateral, similar to the mainshock one. Based on the spatial extent of its own aftershock sequence, on the moment tensor solution, and on the *Wells and Coppersmith (1994)* scaling relation, we propose that the fault plane of the largest aftershock has a strike angle of 336, a dip angle of 86, a rake angle of -11, and a fault surface of 10 by 3.5 km.

2.2 Static Coulomb stress changes calculations

We compute the Static Coulomb stress changes using the fault plane geometry, the rupture, the slip histories and the faulting mechanism adopted by the preliminary model of *Semmane et al., (2004)* that is in good agreement with the relocated seismicity computed by *Fukuyama et al., (2003)*. The geometry of the rupture is described by two planes with different strike angles. The northern fault shows a strike angle of 150, dip angle of 90 and rake angle of 0. The dimensions are set to a length of 16 km and a width of 20 km. The southern fault has a strike angle of 146, dip 90 and rake 0. The dimensions are 16 x 20 km. The hypocenter is located at a depth of 14-15 km. The total fault plane is discretized by a set of 160 square subfaults (2x2km), 80 subfaults for the north-

ern fault and 80 subfaults for the southern fault. Using the Coulomb failure criterion *(Toda and Stein, 2002)* we compute the Coulomb stress change in an elastic halfspace *(Okada, 1992)* by assuming a shear modulus G=3.2 x10^4 MPa and a Poisson's ratio of 0.25. The aim is to resolve the Coulomb stress changes not on Optimally Orientated faults but on planar surface of the known active faults. To this end we consider the fault plane of the largest aftershock of Mw 5.1 (20 km in distance from the fault plane of the mainshock) and we compute there the static coulomb stress changes generated by the mainshock of the fault plane and the slip history calculated by *Semmane et al., (2004)*.

We changed the value of the apparent friction of coefficient μ' to investigate the dependence of the CFF on μ'. We illustrate the results of our computations in the plate 1 where we have considered μ' equal respectively to 0.0, 0.4 and 0.8. We show in these figures the Coulomb stress changes calculated on fault planes having the same mechanism and the same orientation as the plane described previously for the largest aftershock. As we can see, the fault plane of the largest aftershock is located in a stress shadow zone characterized by a negative static stress field, where the seismicity should be inhibited according to the CFF criterion.

The previous computations demonstrate that the static loading alone cannot explain the occurrence of the largest aftershock. We have to consider both dynamic and static loading in a complete Coulomb failure function to explain the occurrence of this peculiar aftershock.

3 Dynamic stress changes after the 2000 Tottori earthquake

3.1 Input parameters

We compute the dynamic stress time histories using the reflectivity method (*Kennet and Kerry, 1979*) and the discrete wavenumber decomposition of the Green's functions (*Bouchon 1981*) as originally proposed by *Cotton and Coutant (1997)*. We image the coseismic stress evolution caused by the fault of the mainshock on the fault plane of the aftershocks in the western region (20 km in distance from the fault plane of the mainshock). We compute both shear and normal stress changes and a time-dependent Coulomb failure function (CFF). We use the fault geometry and the slip history determined by *Semmane et al., (2004)* using a frequency domain inversion procedure *(Cotton and Campillo, 1995)* for the Tottori earthquake. We consider a simple rupture history consisting of a Haskell model with a constant rupture velocity of 2.8 km/s, the nonuniform slip distribution and the rupture times are calculated by *Semmane et al., (2004)*. The source time function is a Bouchon ramp function [f(t)=$\frac{1}{2}$(1+tanh($\frac{t}{\tau}$))], *(Bouchon 1981)*, with a rise time τ of 1.2 s *(Semmane et al., 2004)*. We have computed the stress time histories using a stratified crustal structure used by *Semmane et al., (2004)*. The crustal velocity model is shown in table 1.

We compute the stress evolution on a series of receivers placed at different depths and at different locations on the fault plane of the aftershocks in the western region. This fault plane of interest is parallel to the southern fault and exhibits a dip angle of 86 E. Strike and dip are estimated with the help of the relocated aftershocks of *Fukuyama et al., (2003)*. The fault mechanism is left-lateral strike slip, the same of the mainshock fault. The fault size is estimated from the length of the aftershock area and from the moment magnitude (*Wells*

and Coppersmith 1994).

We have computed the stress components up to a maximum frequency of 1.28 Hz. We decided to discretize the fault plane into a set of 5 by 5 points (Figure 1). On this map the receivers are represented by numbers between 1 and 5 going from north to south. For each receiver we have changed the depth every 1000 m between 3500 m and 7500 m. At each point receiver and for every depth the shear and the normal stress changes on the fault plane of the aftershock have been calculated. Then we can calculate the temporal dependence of the Coulomb stress changes represented by the Coulomb failure function (CFF).

3.2 Results on the fault plane of the largest aftershock

We investigate the influence on the computed Coulomb stress changes of the depth, the apparent friction coefficient and the geographic position on the fault plane of the largest aftershock.

To observe the variation of the CFF with the different values of the apparent friction coefficient, we changed for every simulation μ' between 0.2 and 0.8 fixing the depth and the position of the receiver on the fault. In figure 2, we have computed the stress changes for the point 4 (see fig 1) at a depth of 5250 m, that is the depth for which we have the first aftershock on this fault plane (about 6 hours after the mainshock). This depth is also the hypocentral depth of the largest aftershock. As we can see, the temporal dependence of the coulomb stress changes CFF does not vary a lot by changing μ'. By consequence we will assume μ'=0.4 as widely adopted in the literature. We can explain the independence of the CFF on the apparent coefficient of friction, comparing the shear and the normal stress time histories computed at the same station and at the same depth, as we will describe in the next paragraph.

For each station we have changed the depth between 3500 m and 7500 m, and we have computed the shear, normal and Coulomb stress time histories. The

effective coefficient of friction is 0.4 as in the other simulations. Figure 3 is the result of a simulation computed at the point 4, at the depth of 5250 m. It clearly shows that the normal stress changes are less important than the induced shear stress changes. The shear stress represents the dominant contribution to the Coulomb stress perturbation. This result explain also why the variation of μ' is not important for the Coulomb stress time histories.

The coulomb failure function for every receiver fixing his position on the fault and changing the depth has been computed. For every simulation the depth is respectively equal to 3500m, 4500m, 5250m, 5500m, 6500m, where 5250m is the depth correspondent at the first aftershock on the western fault plane. We report in Figure 4 the case of a station located at point 4. As we can observe, the depth is not a significant parameter for the CFF stress time histories. We can see that by increasing the depth, slightly decrease the two positive peaks of the CFF and slightly increase the negative peak.

In this section, the temporal dependence of the Coulomb stress changes with the location along the fault plane of interest (points 1 to 5) has been investigated. To this end for each simulation the depth and the coordinates (x, y) of the receiver have been fixed. In this study the convention for the axes is that X identifies the direction of the north, Y the direction of the east and Z is downward. The coordinates of theses stations are associated with the red points on Figure 1. For each computation we consider μ'=0.4. 6 different simulations where depth are respectively fixed to 3500m, 4500m, 5250m, 6500m, 7500m and the coordinates change for every simulation between the coordinates of point 1 to the coordinates of point 5 have been computed. In this example the depth is fixed at 5250m and the simulations are computed at the stations located respectively on the point 1-2-3-4-5 of the figure 1. Table 2 reports on the coordinates (x, y) of the stations. Figure 5 presents the results of our computations. We observe a strong dependence of the CFF stress time histories with the different station

locations. This figure shows that as we go from the north to the south, the two positive peaks decrease, the negative peak increases and the static level reaches values smaller and smaller, down to a level of zero static stress eventually becoming negative at the most southern point (point 5). Our results show that the position is more important than the depth and the friction coefficient for the CFF stress time histories. They also show that the shear stress changes have larger amplitudes than the other stress components and hence are the primary control on the evolution of the CFF. The results obtained with this method are consistent with those ones obtained with the static method. Moreover, they provide the time history of stress changes at the locations of interest. In the next section the aim is to calculate the parameters (external loading properties and intrinsic fault properties) that control the triggering of the largest aftershock. Specifically, the aim is to calculate the values of D_c (the critical slip weakening distance of the friction) that could explain the triggering delay of about 48 hours for the largest aftershock of the 2000 Western Tottori earthquake.

4 Estimates of D_c of the largest aftershock

In this section we constrain the fault frictional properties of the largest aftershock of the Tottori earthquake, knowing the state of stress on the fault and the time delay. We consider the triggering of the largest aftershock (M=5.1) that occurred about 48 hours after the mainshock. The static method has shown that the hypocentral area is located into the stress shadow zone characterized by a negative static stress field created by the mainshock, where the seismicity should be inhibited according to the CFF criterion. Therefore we could rule out the possibility of a static triggering of this event. We were compelled to consider then the possibility of a dynamic triggering of this aftershock, 48 hours after the mainshock. Previous studies considered a time delay shorter than a

few minutes, intuitively consistent with the short duration of the dynamic stress changes. Here we consider a time delay of about 48 hours. This time delay can be reduced to 6 hours if we were to consider the first event in the hypocentral area. However, this remains too large for our computing facilities. Moreover, the mechanisms like post seismic relaxation, more probably fluids, may effect the state of stress in the hypocentral area. This is why we have chosen to focus our research on the values of D_c that would lead to a delay that is too short. In this way we are able to rule out all these values and to propose a minimum threshold for D_c that will be consistent with the observed delay.

4.1 Description of the model

In this section we use a finite difference method to approach the problem of the development of an instability on the fault surface. This method is fully described by *Ionescu and Campillo (1999)*. It was adapted to the case of a propagating stress wave by *Voisin et al. (2000)*.

The medium is discretized with a grid step of Δx=Δy=25m. The western fault plane of aftershocks (see fig 1) with a length L embedded in an elastic space is considered. The fault length is set to L=10 km that is also a typical value for a fault segment. This fault dimension is set according to scaling relationships (*Wells and Coppersmith 1994*). The geometry considered on this study is 2D and the field of displacement is antiplane. The shear wave velocity is fixed to c=3000 m/s, the density of the medium is $\rho = 3000$ kg/m^3 and the depth is of 5 km. The normal stress σ_n is assumed to correspond to a depth of 5000 m, that is the depth of the hypocentre of the largest aftershock. We choose a stress drop $\Delta\tau$=11.5 MPa.

Following *Ionescu and Campillo (1999)*, a non-linear slip dependent friction law is considered. The friction law is fully described by τ_s, τ_d, D_c, respectively the static friction, the dynamic friction and the critical slip. The friction law is

nonlinear with respect to the slip displacement u and is given by the following relation (from *Ionescu and Campillo 1999)*:

$$\mu(u) = \mu_s - \frac{\mu_s - \mu_d}{D_c}[u - \frac{D_c}{2\pi} sin(2\pi u/D_c)] \tag{1}$$

The friction decreases from τ_s to τ_d with the ongoing slip (initiation phase) until the slip reaches D_c on some part of the fault (see figure 6). The onset of rupture and the occurrence of triggering corresponds to the end of the initiation phase and to a rupture propagation at the constant residual dynamic stress level. *Ionescu and Campillo (1999)* have shown that the initiation duration is strongly dependent on the slope of friction at the origin, μ' (0). *Ionescu and Campillo (1999)* demonstrated that lower $\mu'(0)$ is, longer the duration of the initiation phese is. The extreme case $\mu'(0)$=0 leads to a vary large initiation duration. Using the finite difference scheme, they carried out experiments with initiation duration of about 100 s. Since our aim is to calculate the friction coefficient that could explain a delay of about some hours, it is interesting for us to consider a non-linear slip dependent friction law to compute the longest time evolution of the fault slip.

The dynamic Coulomb failure function computed in section 4 for the point 5 at a depth of 5250 m (figure 5) is used in this study. As the normal stress dynamic variation is small compared to the shear stress one, we neglect the normal stress variation effect. We assimilate this CFF as the incident shear stress on the fault. The incidence angle of this plane wave is $\theta = 45°$. The stress perturbation is described in figure 5 for the first 35s. The first tiny dynamic stress pulse is reached after 8s, followed by a large negative pulse of -2.5 MPa reached at 11s. Then the large positive pulse of 1.25 MPa is reached at 15s. The static stress field of -0.5 MPa is reached at 20s.

4.2 Triggering delay as a function of the critical slip D_c

We present here the numerical results about the possibility of triggering and also about the timing of triggering as a function of the critical slip D_c. For each value of D_c, we measure the triggering delay between the loading and the eventual rupture. Figure 7 presents the results of this study. The triggering delay is increasing with the value of D_c. This is due to the decrease in the slope of friction with D_c: the characteristic time is increasing. There is no clear difference in the triggering delay for $D_c \leq 0.1$ m. The differences appear when D_c is about 0.3 m. Above this value it becomes impossible to trigger the faults within a few minutes. Therefore, we can conclude that in order to avoid an immediate or quasi-immediate triggering delay, the critical slip-weakening distance must be greater than 0.3m.

5 Discussion

5.1 Friction law and aftershock triggering

Two friction laws are classically used in the community, both based on laboratory experiments. On one hand, the rate and state friction law (*Dieterich, 1992*) that describes the stick-slip experiments and aftershock triggering by positive static stress changes (*Dieterich, 1994*). On the other hand, the slip-dependent friction law (e.g. *Ohnaka et al., 1987*) describes the short time initiation of rupture. It is used for dynamic rupture simulations (e.g. *Ida, 1972, Andrews, 1976, Day, 1982*), much less to investigate aftershock triggering (*Voisin et al., 2000, 2004*).

We classically distinguish between static and dynamic stress triggering. The Rate and State friction law predicts a seismicity rate increase in regions of static stress increase, and a seismicity rate decrease in regions of static stress decrease. Dynamic triggering of remote seismicity appears like the shortcoming of the the-

ory. Recent studies (e.g. *Belardinelli et al. 2003*) demonstrate that dynamic stress waves may have an "instantaneous triggering effect" under the condition that it overcomes the direct friction effect. This is in conflict with direct observations of remote seismicity triggered by large earthquakes, that occur at the time of the waves passage but also well after. *Parsons [2005]* proposes that the dynamic stress waves change the mean critical slip distance at nucleation zones, leading to delayed instability and Omori's law. Similarly, the SD friction law allows for an immediate or a delayed instability triggered by the dynamic stress waves. The results presented in *Voisin et al. 2004* have demonstrated that the effect of dynamic stress waves is finite in time, although it is difficult to infer the maximum triggering delay we can expect because of the computational techniques. A maximum delay of 2 minutes was reached using a finite difference scheme by *Voisin 2002*. This was extended using a finite element method up to half an hour in *Voisin et al. 2002*. This is nothing compared to the characteristic time of evolution of a fault under a Rate and State friction law, typically as large as 100 years. Can we expect larger time delays for dynamic triggering? The 1992 Landers-Little Skull Mountain couple of earthquakes provides an example of dynamic triggering delay of 22 hours (*Bodin and Gomberg, 1994; Gomberg and Bodin, 1994*). Answer to that question could be possible if we were able to consider the complete stress perturbation, the fault geometry, the friction parameters and the initial state of stress on the fault plane. So far, this is out of reach. By consequence we cannot reject the hypothesis that the largest aftershock of the 2000 Western Tottori earthquake has been triggered by dynamic stress waves.

5.2 Value of D_c for the largest aftershock

As explained above, we have followed the methodology used in *Voisin et al. 2000* to infer the fault frictional properties. Assuming the fault geometry and

the state of stress on the aftershock fault plane, we use the time delay between the dynamic loading and the eventual triggering of the aftershock. In the case of the largest aftershock of the 2000 Tottori earthquake, our goal is not to give a complete set of frictional parameters that can explain a triggering delay of 48 hours. It rather consists in determining the threshold in D_c that leads to large delays. Doing so, we have obtained a minimum value for D_c of 0.3 meters. This seems quite large, especially for an aftershock of magnitude 5.1. However, one must recall that we have set the prestress on the fault to unity, which simply means that everywhere on the fault the initial stress equals the fault strength. For the sake of simplicity, the fault plane that we have considered is homogeneous. We know from previous studies that this value for D_c must be understood as an apparent value of the critical slip weakening distance accounting for small scale heterogeneities (*Campillo et al., 2001; Voisin et al., 2002*). The actual value of D_c might be much smaller than 0.3 m. This value of D_c is consistent with those of other seismological studies that have been computed with differents methods. Many differents approaches have been proposed to estimate the critical slip weakening distance (D_c) for real earthquakes. *Olsen et al. (1997)* and *Peyrat et al. (2001)* found D_c on the order of 80 cm from waveform inversion of the accelerograms observed during the 1992 Landers earthquake, with spontaneous dynamic rupture models. Recently *Mikumo et al. (2003)* have estimated the value of D_c from strong-motion records by using a new approach, independently from the estimate of the fracture energy or radiated seismic energy. This approach is based on the estimate of the slip weakening distance at each point on the fault as the slip D_c' at the time of peak slip-velocity, using a slip-weakening friction law. For the 2000 Tottori and the 1999 Kobe events it was found that D_c ranges between 40 and 90 cm. The theoretical demonstration of this approach is discussed in (*Fukuyama et al., 2003*). They have shown that the estimates of D_c' can be affected by an error of roughly 50 percent. *Tinti et*

al., (2004) generalized the results of *Fukuyama et al., 2003* and showed that the estimated value of the parameter D'_c is affected by the adopted friction law and the constitutive parameters. They found that the differences between D'_c and D_c can vary from few percent up to 50 percent. Estimates of D_c by differents means are always quite large (1m) when compared to values derived from laboratory experiments (10 μm). This, with other considerations, may suggest that D_c is scale-dependent. However, our approach leads us to consider an effective representation of the fault that integrates small-scale heterogeneities (*Campillo et al.,2001; Voisin et al., 2002*). By consequence the values of D_c that we derive from our analysis are understood as "apparent" D_c.

5.3 Implications for seismic hazard

The static stress transfer theory favors the idea that the largest aftershock should occur in an area of increased Coulomb stress change. The most publicized example of such a case is given by the 1992 Landers-Big Bear earthquakes (*King et al. 1994*). The 2000 Western Tottori earthquake provides an interesting counterexample of when and where the largest aftershock can occur. If we consider the Coulomb stress change on optimally oriented faults, the largest aftershock has occurred in an area of increased Coulomb stress change. However, since its fault mechanism is left lateral strike slip, if we compute the Coulomb stress change on this particular fault orientation with this particular mechanism, the largest aftershock has occurred in an area of decreased Coulomb stress change (plate 1). Any attempt to forecast the major aftershocks based on the static Coulomb stress changes would have missed this aftershock.

Determining which of dynamic or static stresses is the most relevant to near-field triggering is an important issue for earthquake probability forecasts (*Parsons, 2005*).

6 Conclusions

We focused on the 2000 Western Tottori (Japan) earthquake (M 6.6 6.8) and on the triggering of its largest aftershock (M 5.1). The static stress transfer computations show that the Coulomb stress was decreased on the particular fault plane. Therefore this largest aftershock should have not occured. Yet it was triggered 48 hours after the mainshock. We have computed the complete Coulomb Failure Function for the hypocentral area of the largest aftershock. We conclude that to explain the occurrence of this aftershock it is not sufficient to account only for the static stress field but it is essential to consider the complete Coulomb failure function that includes static and dynamic stress perturbations. The hypothesis of a dynamic triggering of this largest aftershock cannot be rejected despite the large triggering delay. Using a finite difference method, we are able to set a minimum value for the critical slip distance on the fault plane of the aftershock: 0.3m. Below this value, the largest aftershock would have occurred within minutes of the mainshock. On a timescale of a few hours to a few day, other processes like poroelasticity, or other fluid effects, may affect the state of stress in the hypocentral area of the aftershock. Therefore, we cannot conclude on the hypothesis of a purely dynamic triggering of this aftershock. Dynamic stress waves have certainly promoted the failure by some process that was relayed by others like poroelasticity. The question is now, if possible, to set an upper limit on the time efficiency of the dynamic triggering. One minute? One hour? One day? One month? The triggering of the largest aftershock of the 2000 Western Tottori earthquake provides an argument in favour of at least a one day lasting effect.

By Sara Di Carli [(1)], Christophe Voisin, Fabrice Cotton, Fethi Semmane
Laboratoire de Géophysique Interne et Tectonophysique, Observatoire des Sciences de l'Univers de Grenoble, Université Joseph Fourier, BP 53, F-38041 Grenoble, France.
(1) Now at Laboratoire de Géologie, Ecole Normale Superieure, 24 rue Lhomond, 75231 Paris Cedex 05, France.
(e-mail: sdicarli@geologie.ens.fr, cvoisin@obs.ujf-grenoble.fr, fcotton@obs.ujf-grenoble.fr, fsemmane@obs.ujf-grenoble.fr)

References

[1] Aki, K., and Richards, P.G., (1980), Quantitative Seismology, vol.2, 932 pp., W.H. Freeman, New York.

[2] Andrews, D.J., (1976), Rupture propagation with finite stress in antiplane strain, *Bull. Seismol. Soc. Am.*, 81, 3575-3582.

[3] Belardinelli M. E., Cocco M., Coutant O., Cotton F., (1999), Redistribution of dynamic stress during coseismicruptures: Evidence for fault interaction and earthquake triggering, *J. Geophys. Res., 104*, 14,925-14,945.

[4] Belardinelli, M.E., Bizzarri, A., Cocco, M., (2003), Earthquake triggering by static and dynamic stress changes, *J. Geophys. Res.*, 108(B3),2135, doi:10.1029/2002JB001779

[5] Bodin P., J., Gomberg, (1994), Triggered seismicity and deformation between the Landers, California, and Little Skull Mountain, Nevada, earthquakes, *Bull. Seism. Soc. Am.*, 84, 835-843.

[6] Bouchon M., (1981), A simple method to calculate Green's function for layered media, *Bull. Seism. Soc. Am.*, 71.959-971.

[7] Brodsky, E., V. Karakostas, and H. Kanamori, (2000), A new observation of dynamically triggered regional seismicity: Earthquakes in Greece following the August, 1999 Izmit, Turkey earthquake, *Geophys. Res. Lett.*, 27,2741-2744.

[8] Campillo, M., P. Favreau, I. Ionescu, and C. Voisin, (2001), On the effective friction law of an heterogeneous fault, *J. Geophys. Res.,* 106, 16,237-16,250.

[9] Cotton F., Coutant O., (1997), Dynamic stress variations due to shear faults in a plane-layered medium, *J. Geophys. Int.*, 128, 676-688.

[10] Cotton F., Campillo M., (1995), Frequency domain inversion of strong motions: Application to the 1992 Landers earthquake, *J. Geophys. Res.*, 100, 3961-3975.

[11] Dalguer, L., K. Irikura, W. Zhang, and J.D. Riera (2002), Distribution of dynamic and static stress changes during 2000 Tottori (Japan) earthquake: Brief interpretation of the earthquake sequences; foreshocks, mainshock and aftershocks, *Geophys. Res. Lett.*, 29(16), 1758, doi:10.1029/2001GL014333

[12] Day, S. M., (1982), Three-dimensional finite difference simulation of fault dynamics: Rectangular faults with fixed rupture velocity, *Bull. Seismol. Soc. Am.*,72, 705-727.

[13] Dietrich, J.H., (1992), Earthquake nucleation on faults with rate-and state-dependent strength, *Tectonophysics*, 211, 115-134.

[14] Dietrich, J.H., (1994), A constitutive law for rate of earthquake production and its application to earthquake clustering, *J. Geophys. Res.*, 99, 2601-2618.

[15] Fukuyama E., Ellsworth W.L., Waldhauser F., Kubo A., (2003), Detailed Fault Structure of the 2000 Western Tottori, Japan, earthquake sequence, *Bulletin of the Seismological Society of America*, *93*, 1468-1478.

[16] Fukuyama, E., T. Mikumo, and K. B. Olsen (2003). Estimation of critical slip-weakening distance: its theoretical background, *Bull. Seism. Soc. Am.*, 93, 1835-1840.

[17] Glowacka-E; F. A. Nava; G.D. de Cossio; V. Wong; and F. Farfan, (2002), Fault slip, seismicity, and deformation in Mexicali Valley, Baja California, Mexico, after the M 7.1 1999 Hector Mine earthquake, *Bulletin of the Seismological Society of America*, 92, 1290-1299.

[18] Gomberg, J., P.A. Reasenberg, P. Bodin, and R.A. Harris, (2001), Earthquake triggering by seismic waves following the Landers and Hector Mine earthquakes, *Nature*, 411, 462-466.

[19] Gomberg, J., and P. Bodin, (1994), Triggering of the Ms=5.4 Little Skull Mountain, Nevada, earthquake with dynamic strain, *Bull. Seism. Soc. Am.*, 84, 844-853.

[20] Gomberg, J., P. Bodin, and P. A. Reasenberg, (2003), Observing earthquakes triggered in the near-field by dynamic deformations, *Bull. Seism. Soc. Am.*, 93, 118-138.

[21] Hill, D. P., P. A. Reasenberg, A. Michael, W.J. Arabaz, and G.C. Beroza, (1993), Seismicity remotely triggered by the magnitude 7.3 Landers, California, earthquake, *Science*, 260, 1617-1623.

[22] Husen, S., Taylor, R., Smith, R. B., and Healser H., (2004), Changes in geyser eruption behavior and remotely triggered seismicity in Yellowstone National Park produced by the 2002 M 7.9 Denali fault earthquake, Alaska, *Geology*, V. 32; no. 6; p. 537-540; DOI: 10.1130/G20381.1

[23] Ida, Y., (1972), Cohesive force across the tip of a longitudinal-shear crack and Griffith's specific surface energy, *J. Geophys. Res.*, 77, 3796-3805.

[24] Ionescu, I., and M. Campillo, (1999), Influence of the shape of friction law and fault finiteness on the duration of initiation, *J. Geophys. Res., 104,* 3013-3024.

[25] Iwata, T., and H. Sekiguchi, (2001), Substance of the earthquake faulting during the 2000 western Tottori earthquake, *SEISMO 5*,5-7(in Japanese).

[26] Iwata, T., and H. Sekiguchi, (2002), Source process and near-source ground motion during the 2000 Tottori-ken Seibu earthquake, *Proc.11th Japan Earthqu. Eng. Symp.*, 125-128 (in Japanese with English abstract).

[27] Kadinski-Cade, K., and R. J. Willemann, (1982), Towards understanding aftershock patterns: the basic pattern for strike-slip earthquakes, *EOS Trans.*, AGU, 63, 384.

[28] Kanamori, H., (1972), Determination of effective tectonic stress associated with earthquake faulting, the Tottori earthquake of 1943, *Phys. Earth Planet. Interiors*, 5, 426-434.

[29] Kennet, B. L. and Kerry, N.J., (1979) Seismic waves in a stratified half space, *Geophys. J. R.astr; Soc.*, 57, 557-583.

[30] Kilb, D., (2003), A strong correlation between induced peak dynamic coulomb stress change from the 1992 M 7.3 Landers, California, earthquake and he hypocenter of the 1999 M 7.1 Hector Mine, California, earthquake, *J. Geophys. Res.*, 108(B1), 2012, doi: 10.1029/2001JB000678.

[31] Kilb, D., J. Gomberg, and P. Bodin, (2000), Earthquake triggering by dynamic stresses, *Nature*, 408, 570-574.

[32] Kilb, D., J. Gomberg, and P. Bodin, (2002), Aftershock triggering by complete Coulomb stress changes, *J. Geophys. Res.*, 107(B4), 2060, doi: 10.1029/2001JB000202.

[33] Kilb, D., J. Gomberg, and P. Bodin, (1999), Complete coulomb failure stress changes and earthquake triggering, (abstract), *Eos Trans*, Agu, 80(46), Fall Meet. Suppl., F1005-F1006.

[34] King, G. C. P., Stein, R. S., and Lin, J., (1994), Static stress changes and the triggering of earthquakes, *Bull. Seismol. Soc. Am.*, 84, 935-953.

[35] Mikumo, T., Olsen K. B., Fukuyama, E., and Yagi Y., (2003), Stress-Breakdown Time and Slip-Weakening Distance Inferred from Slip-Velocity Functions on Earthquake Faults, *BSSA*, Vol. 93, No. 1, pp. 264-282

[36] Okada, Y., (1992), International deformation due to shear and tensile faults in an half-space, *Bull. Seism. Soc. Am.*, 82, 1018-1040.

[37] Ohnaka, M., Y. Kuwahara, and K. Yamamoto, (1987), Constitutive relations between dynamic physical parameters near a tip of the propagating slip zone during stick-slip shear failure, *Tectonophysics, 144*, 109-125.

[38] Olsen, K. B., R. Madariaga, and R.J. Archuleta (1997), Three-dimensional dynamic simulation of the 1992 Landers earthquake, *Science*, 278, 834-838.

[39] Parsons, T., (2005), A hypothesis for delayed dynamic earthquake triggering, *Geophysical Research Letters*, Vol. 32, L04302, doi:10.1029/2004GL021811.

[40] Peyrat, S., K. B. Olsen, and R. Madariaga (2001), Dynamic modeling of the 1992 Landers earthquake, *J. Geophys. Res.*, 106, 26,467-26,482.

[41] Peyrat, S., and K. B. Olsen (2004), Nonlinear dynamic rupture inversion of the 2000 Western Tottori, Japan, earthquake, *Geophys. Res. Lett.*, 31, L05604, doi:10.1029/2003GL019058.

[42] Pulido N. and Irikura K.(2000), Estimation of Dynamic Rupture Parameters from the Radiated Seismic Energy and Apparent Stress, *Geophys. Res. Lett.*, VOL. 27, NO. 23, PAGES 3945-3948.

[43] Sagiya, T., T., Nishimura, Y. Hatanaka, E. Fukuyama, and W. L. Ellsworth, (2002), Crustal movements associate with the 2000 western Tottori earthquake and its fault models, *Zisin, (J. Seismol. Soc. Jpn)*, Ser. 54, 523-534 (in Japanese with English abstract).

[44] Semmane, F., F. Cotton, and M. Campillo, (2004), The 2000 Tottori earthquake: A large shallow earthquake without any superficial rupture. EGU 1st meeting, Nice, France, 25-30 April 2004.

[45] Shibutani, T., S. Nakao, R. Nishida, F. Takeuchi, K. Watanabe, and Y. Umeda, (2002), Swarm-like seismic activity in 1989, 1990, and 1997 preceding the 2000 Western Tottori earthquake, *Earth Planets Space* 54, 831-845.

[46] Stein, R. S., and M. Lisowski, (1983), The 1979 Homestead Valley Earthquake Sequence, California: Control of aftershocks and Postseismic Deformation, *Journal of Geophysical Research*, 88, 6477-6490.

[47] Stein, R.S., King, G. C. P., Lin, J.,(1999), Stress transfer in earthquake occurrence, *Nature* 402, December.

[48] Stein, R. S., King, G. C. P., Lin, J., (1992), Change in failure stress on the southern San Andreas fault system caused by the 1992 Magnitude=7.4 Landers earthquake, *Science* 258, 1328-1332.

[49] Tinti E., Bizzarri A., Piatanesi A., and Cocco M., (2004), Estimates of slip weakening distance for different dynamic rupture models, *Geophysical Research Letters*, VOL.31, L02611, doi:10.1029/2003GL018811.

[50] Toda S., Stein R. S., (2002), Reponse of the San Andreas fault to the 1983 Coalinga-Nunez Earthquake: An application of interaction-based probabilities for Parkfield, *J. Geophys. Res.*, 107,10.1029/2001JB000172.

[51] Toda S., R. S. Stein, P. A. Reasenberg, J. H. Dietrich, and A. Yoshida, (1998), Stress transferred by the 1995 Mw=6.9 Kobe, Japan, shock: Effect on aftershocks and future earthquake probabilities, *J. Geophys. Res.*, 103(B10), 24, 543-24, 565.

[52] Voisin C., Cotton F., Di Carli S., (2004) A reconciling model for dynamic and static stress triggering of aftershocks, antishocks, remote seismicity, creep events and multisegmented rupture, *Journal of Geophysical Research*, *109*, B06304, doi: 10.1029/2003JB002886

[53] Voisin C., Campillo M., Ionescu I.R., Cotton F., Scotti O., (2000), Dynamic versus static stress triggering and friction parameters: Inferences from the November 23, 1980, Irpinia earthquake, *J. Geophys. Res.*, VOL.105, NO.B9, 21, 647-21, 659.

[54] Voisin C., I. R. Ionescu, M. Campillo, R. Hassani, and Q.L. Nguyen, (2002), Process and signature of initiation on a finite fault system: a spectral approach, *J. Geophys. Res.*, *148*, 120-131.

[55] Wells, D.L. and Coppersmith, K.J., 1994. New empirical relationships among magnitude, rupture length, rupture width, rupture area, and surface displacement. *BSSA*, 84: 974 - 1002.

[56] Yagi, Y., and M. Kikuchi,(2000), Source process of the 2000 October 6 Western Tottori Earthquake (preliminary report), *Newslett. Seism. Soc. Jpn.*,12, no.4,9-10, (in Japanese).

7 Figure Captions

Figure1. The map shows the fault geometry adopted in our computations and the relocated aftershocks. The red points represent the virtual receivers placed on the fault plane of the largest aftershock.

Plate1. Coulomb stress map computed for the specific fault mechanism of the largest aftershock. a/ The apparent friction coefficient is set to 0.0. b/ The apparent friction coefficient is 0.4. c/ The apparent friction coefficient is 0.8.

Figure2. Coulomb failure function (CFF) time histories calculated at the station 4 and at a depth of 5250 m, for different friction coefficients μ', equal to 0.2, 0.4, 0.6, 0.8.

Figure3. Coulomb failure function, normal stress and shear stress time histories calculated at the station 4 for a depth of 5250 m.

Figure4. Coulomb failure function (CFF) time histories at the station 4 for different values of the depth, equal respectively to 3500m, 4500m, 5250m, 5500m, 6500m.

Figure5. Coulomb failure function (CFF) time histories calculated respectively at the station 1, 2, 3, 4, 5, for a depth of 5250m.

Figure6. Nonlinear friction laws used in this study. The friction decreases from μ_s down to μ_d with the ongoing slip (initiation phase). As the slip reaches D_c, the friction stabilizes at the residual dynamic level (propagation phase). The parameter p allows for a change in the initial slope of the friction law.

Figure7. Triggering delay as a function of the critical slip distance D_c. The values of the critical slip D_c that range from 0.01 to 0.3 m are not acceptable to explain the delay of about 6 hours. The values acceptable are for $D_c \geq 0.3$ m.

Depth (km)	V_p (km/s)	V_s (km/s)	ρ (kg/m^3)	Q_p	Q_s
0	5.50	3.179	2600	500	200
2	6.05	3.497	2700	500	200
16	6.60	3.815	2800	500	200
38	8.03	4.624	3100	500	200

Table 1:

stations	x	y	z
station1	-1499.28	-25767.99	5250.00
station2	-6050.78	-23781.90	5250.00
station3	-10945.29	-23130.00	5250.00
station4	-13581.83	-18865.05	5250.00
station5	-18946.24	-15737.26	5250.00

Table 2:

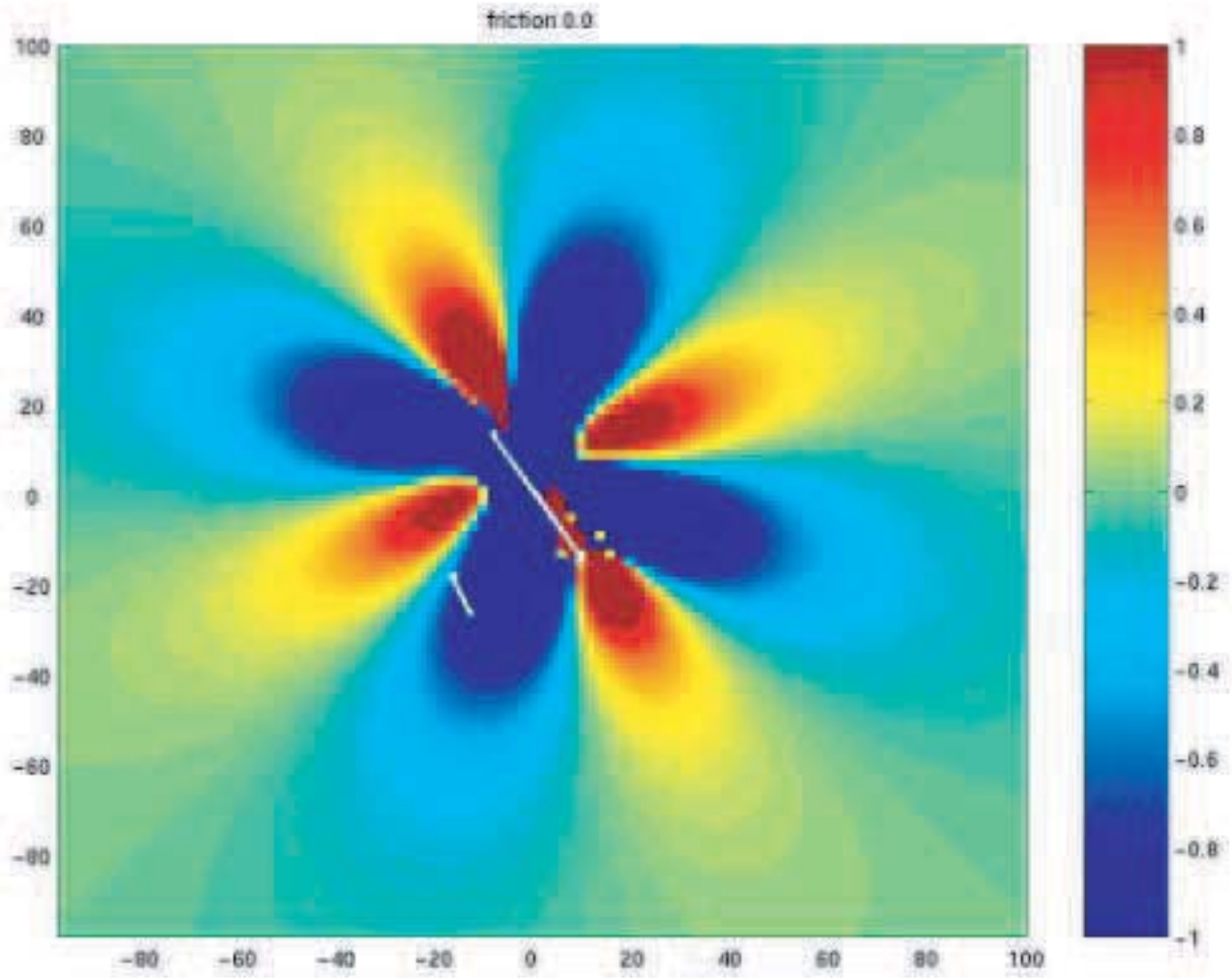
friction 0.0
100
80
60
40
20
0
-20
-40
-60
-80
-80
-60
-40
-20
0
20
40
60
80
100
1
0.8
0.6
0.4
0.2
0
-0.2
-0.4
-0.6
-0.8
-1

Plate a)

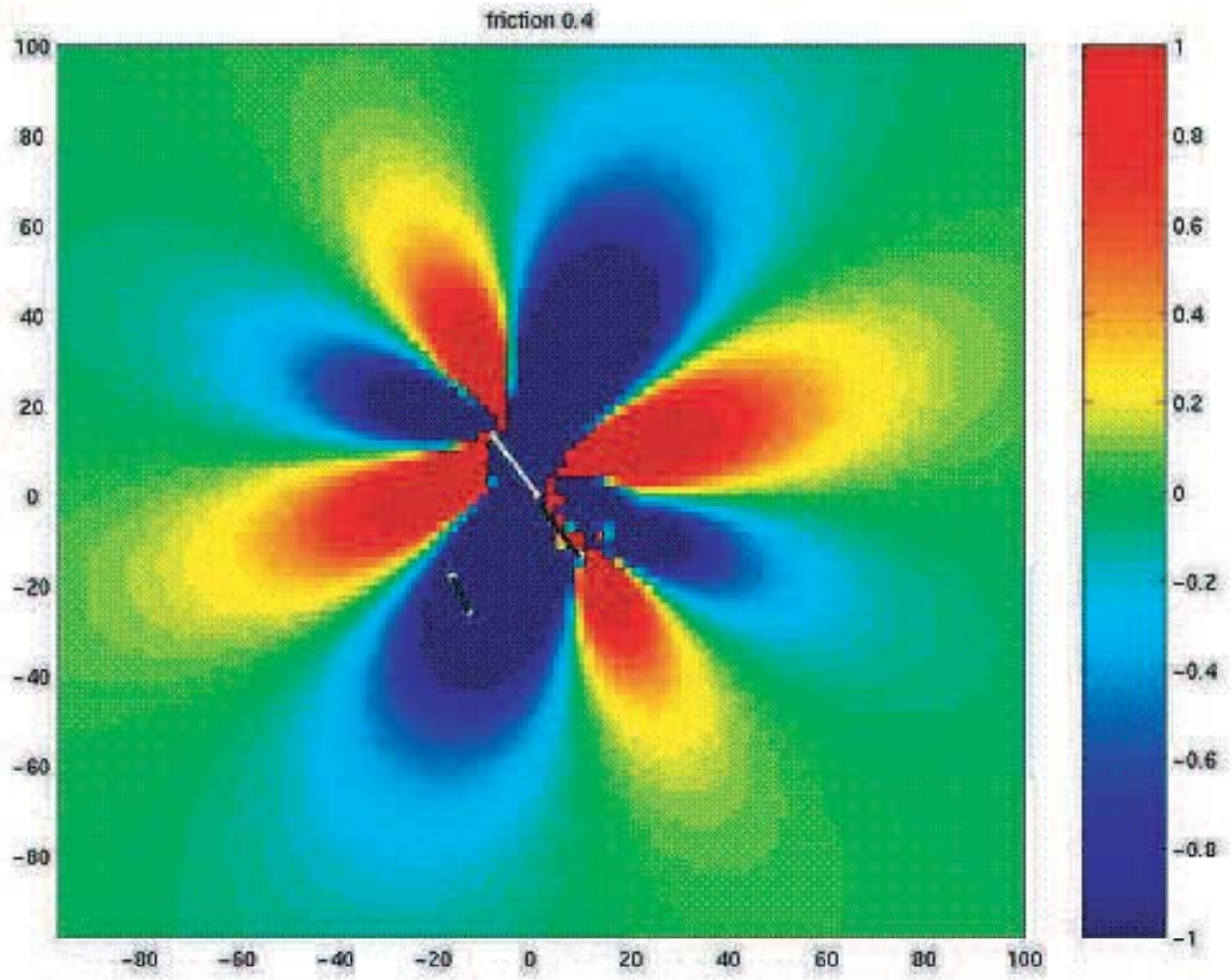
friction 0.4
100
80
60
40
20
0
-20
-40
-60
-80
-80
-60
-40
-20
0
20
40
60
80
100
1
0.8
0.6
0.4
0.2
0
-0.2
-0.4
-0.6
-0.8
-1

Plate b)

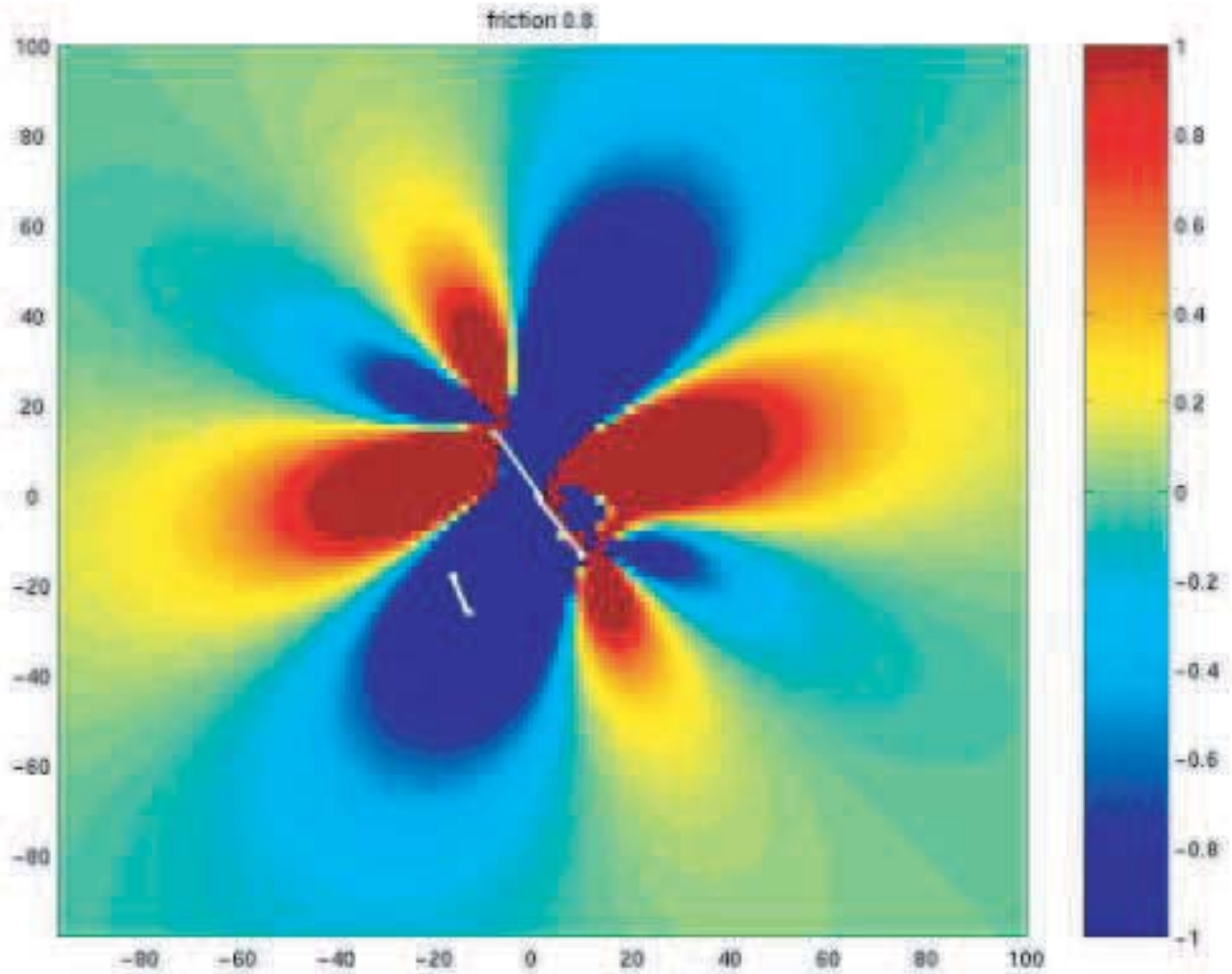
friction 0.8
100
80
60
40
20
0
-20
-40
-60
-80
-80
-60
-40
-20
0
20
40
60
80
100
1
0.8
0.6
0.4
0.2
0
-0.2
-0.4
-0.6
-0.8
-1

Plate c)

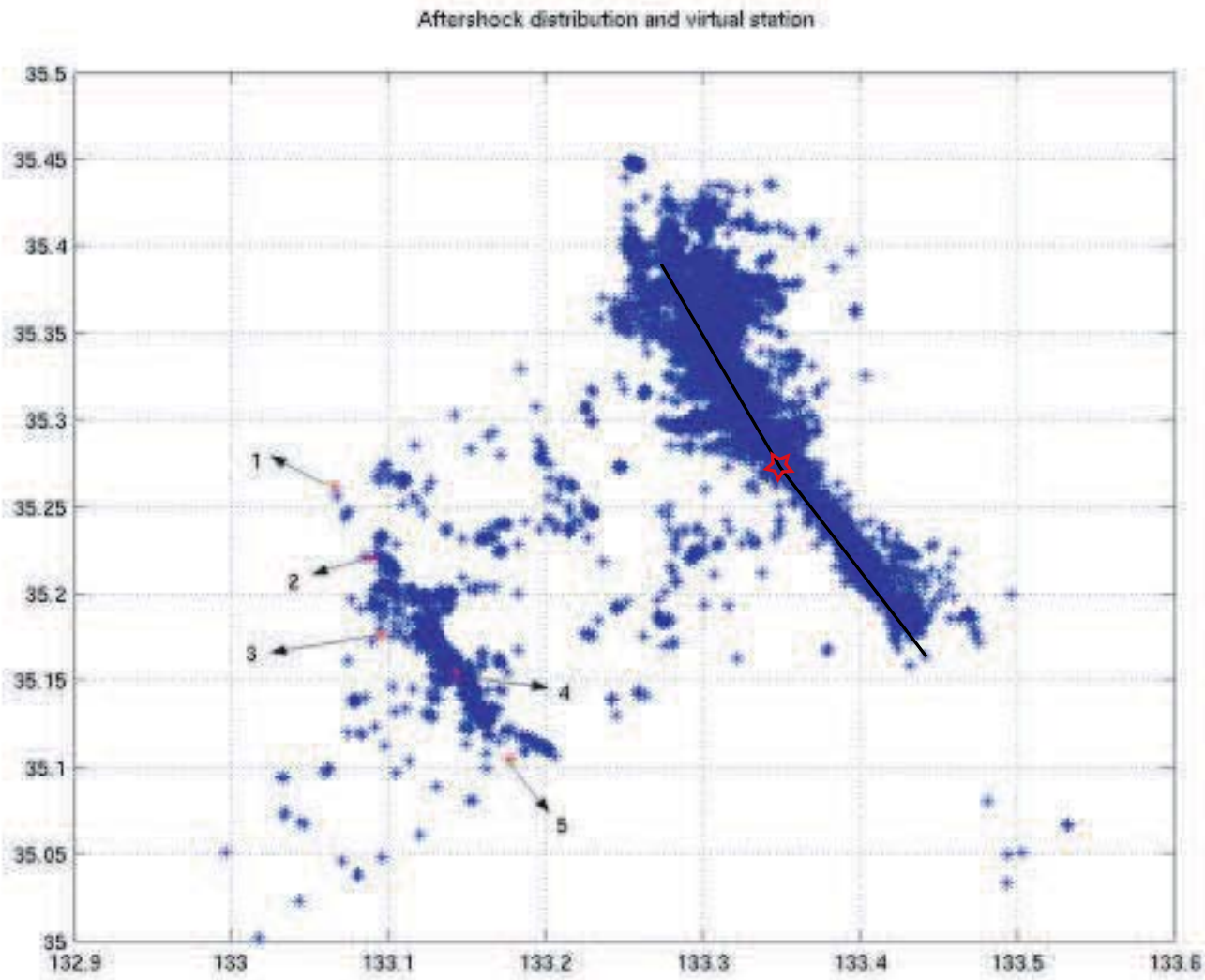
Aftershock distribution and virtual station
35.5
35.45
35.4
35.35
35.3
35.25
35.2
35.15
35.1
35.05
35
132.9
133
133.1
133.2
133.3
133.4
133.5
133.6
1
2
3
4
5

Figure 1:

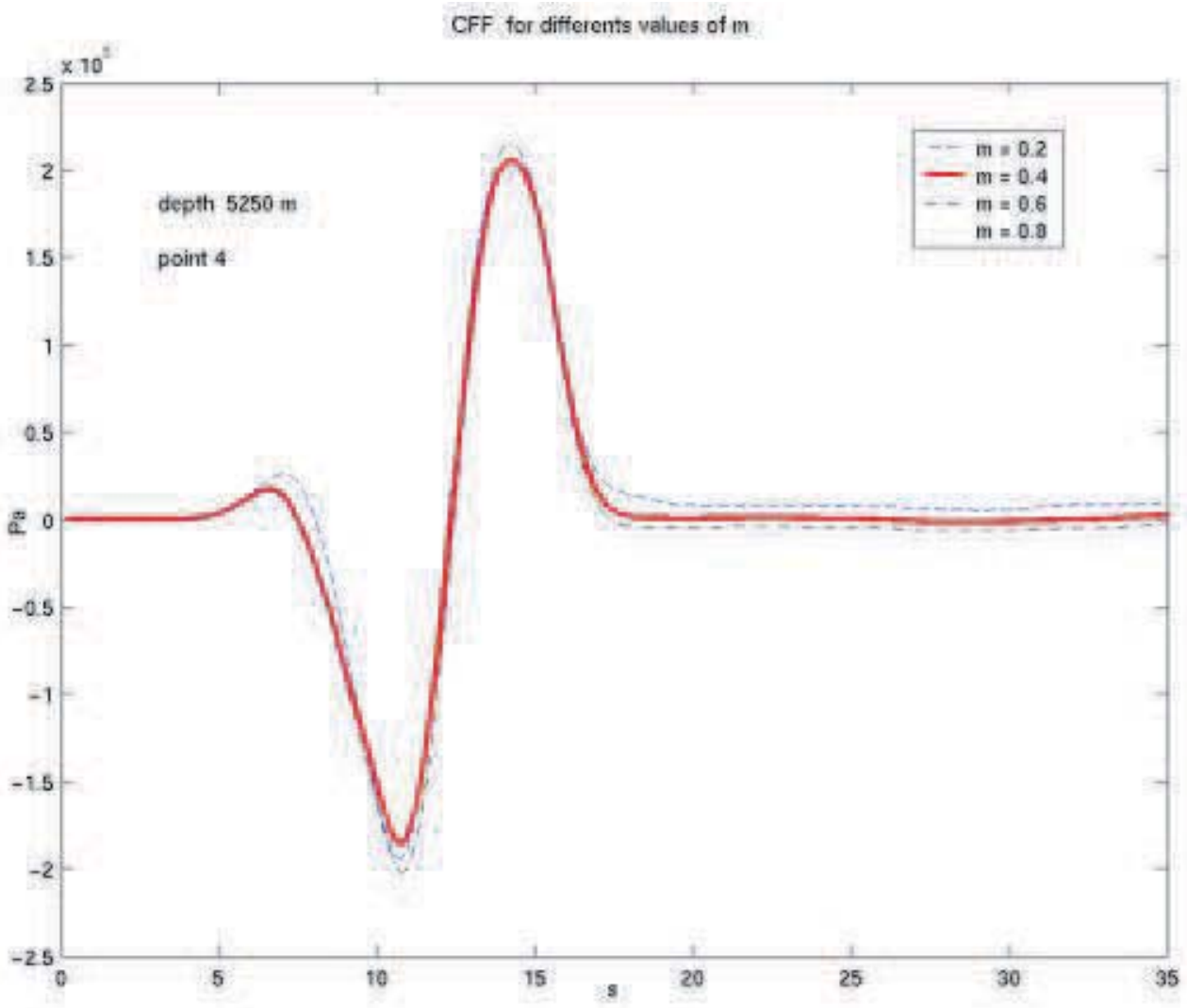
CFF for differents values of m
x 10
depth 5250 m
point 4
m = 0.2
m = 0.4
m = 0.6
m = 0.8
Pa
s
2.5
2
1.5
1
0.5
0
-0.5
-1
-1.5
-2
-2.5
0
5
10
15
20
25
30
35

Figure 2:

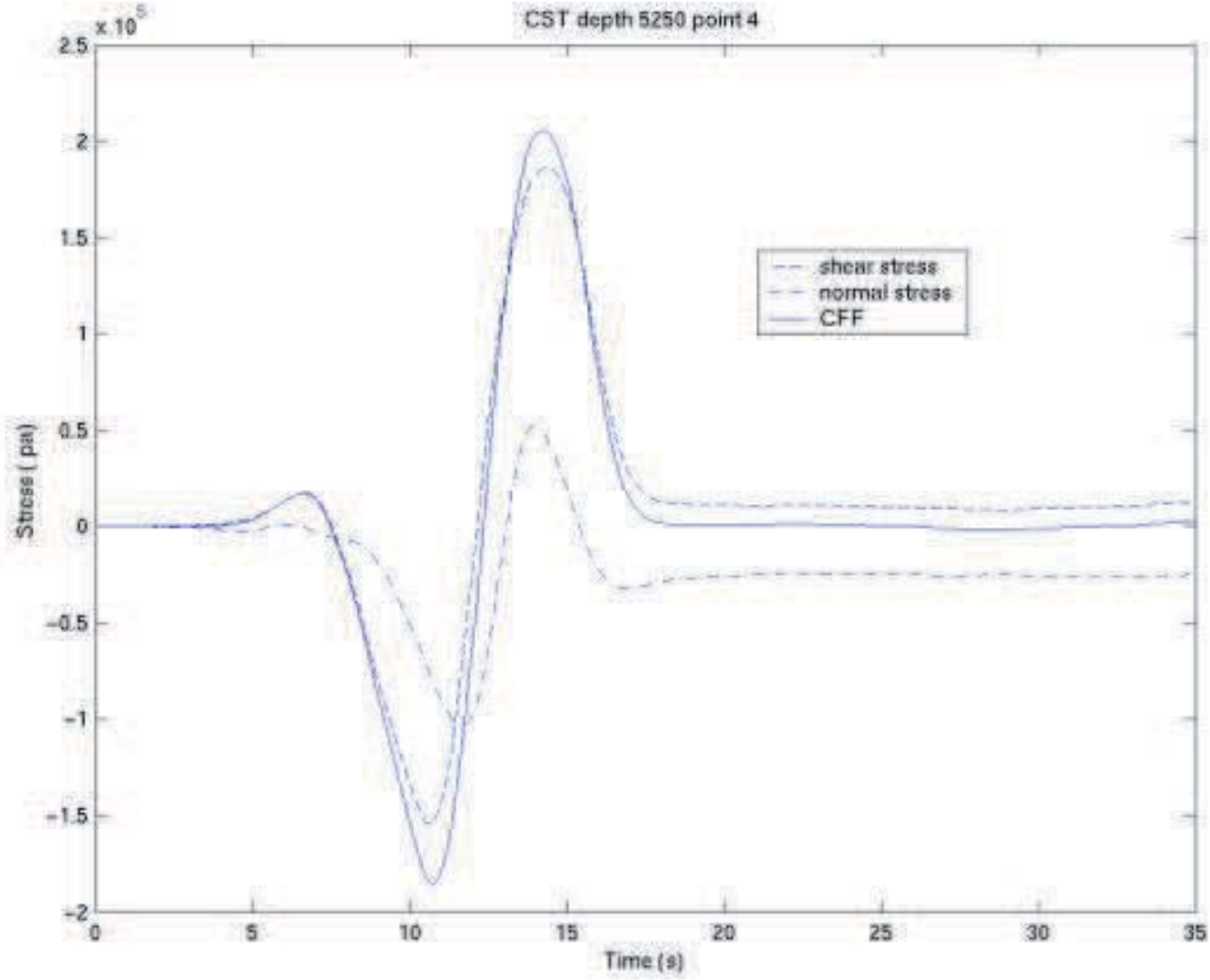
CST depth 5250 point 4
x 10^5
2.5
2
1.5
1
0.5
0
-0.5
-1
-1.5
-2
Stress (pa)
0
5
10
15
20
25
30
35
Time (s)
shear stress
normal stress
CFF

Figure 3:

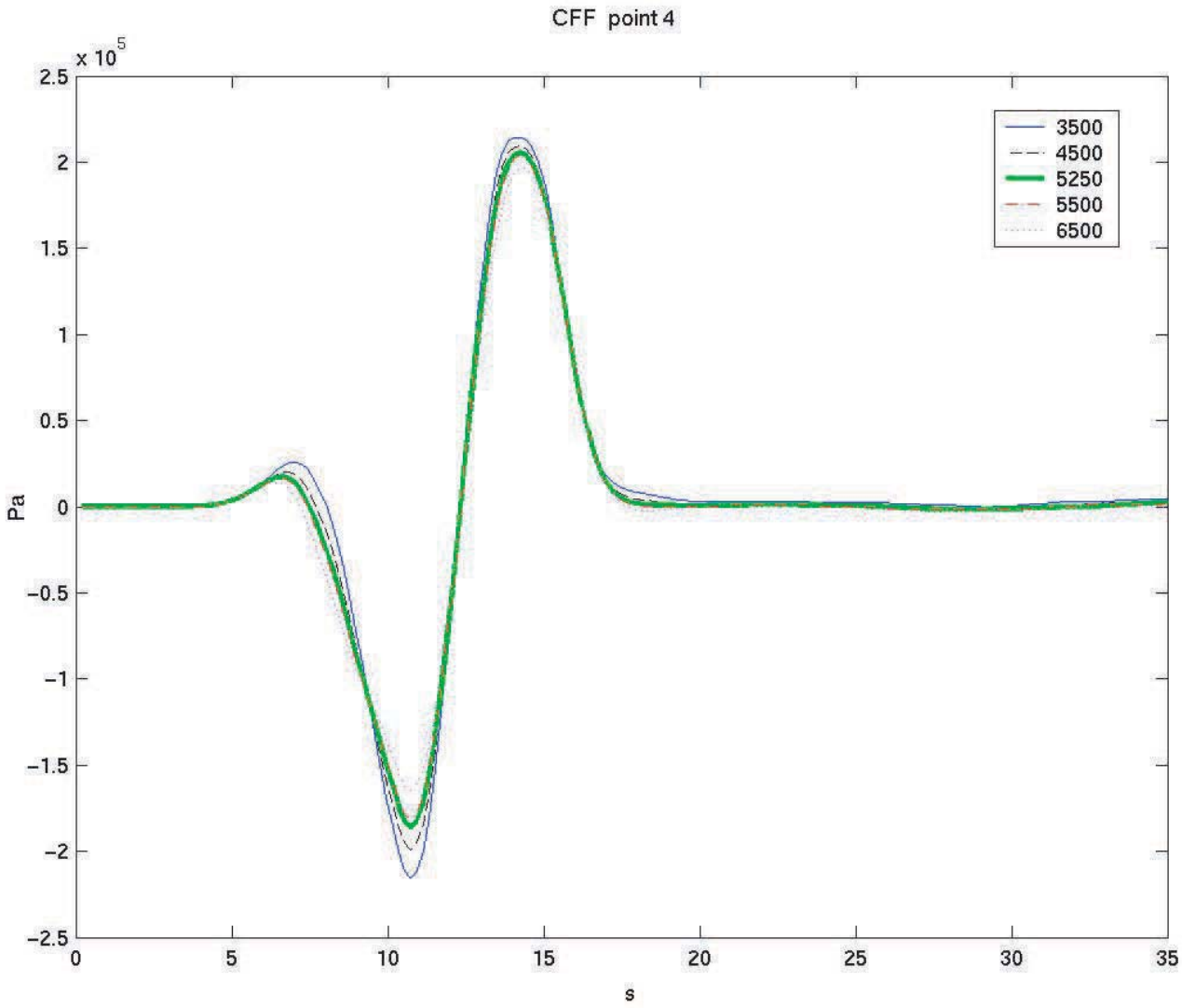
CFF point 4
x 10^5
2.5
2
1.5
1
0.5
0
−0.5
−1
−1.5
−2
−2.5
Pa
0
5
10
15
20
25
30
35
s
3500
4500
5250
5500
6500

Figure 4:

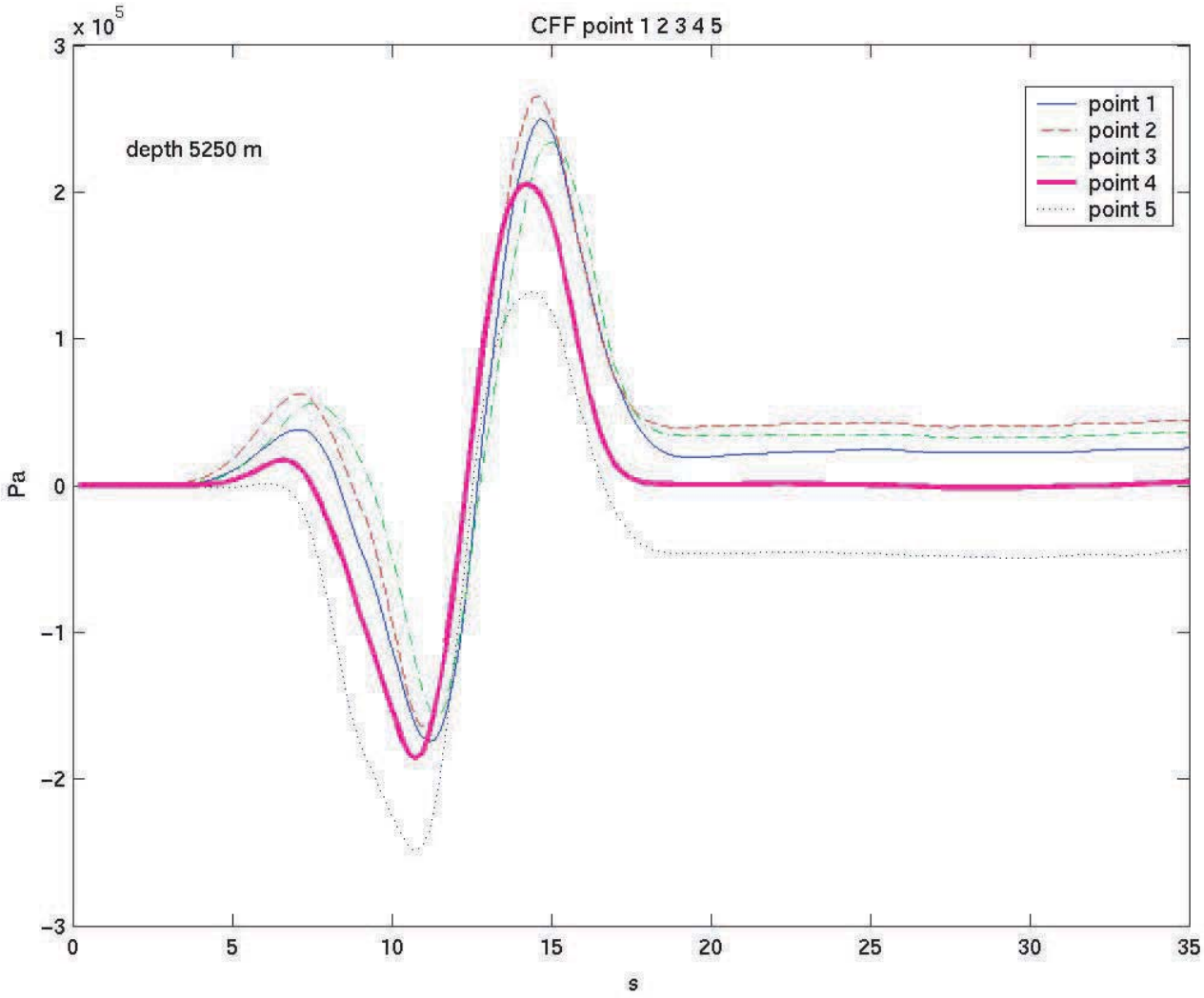
x 10^5
CFF point 1 2 3 4 5
depth 5250 m
point 1
point 2
point 3
point 4
point 5
Pa
s
3
2
1
0
−1
−2
−3
0
5
10
15
20
25
30
35

Figure 5:

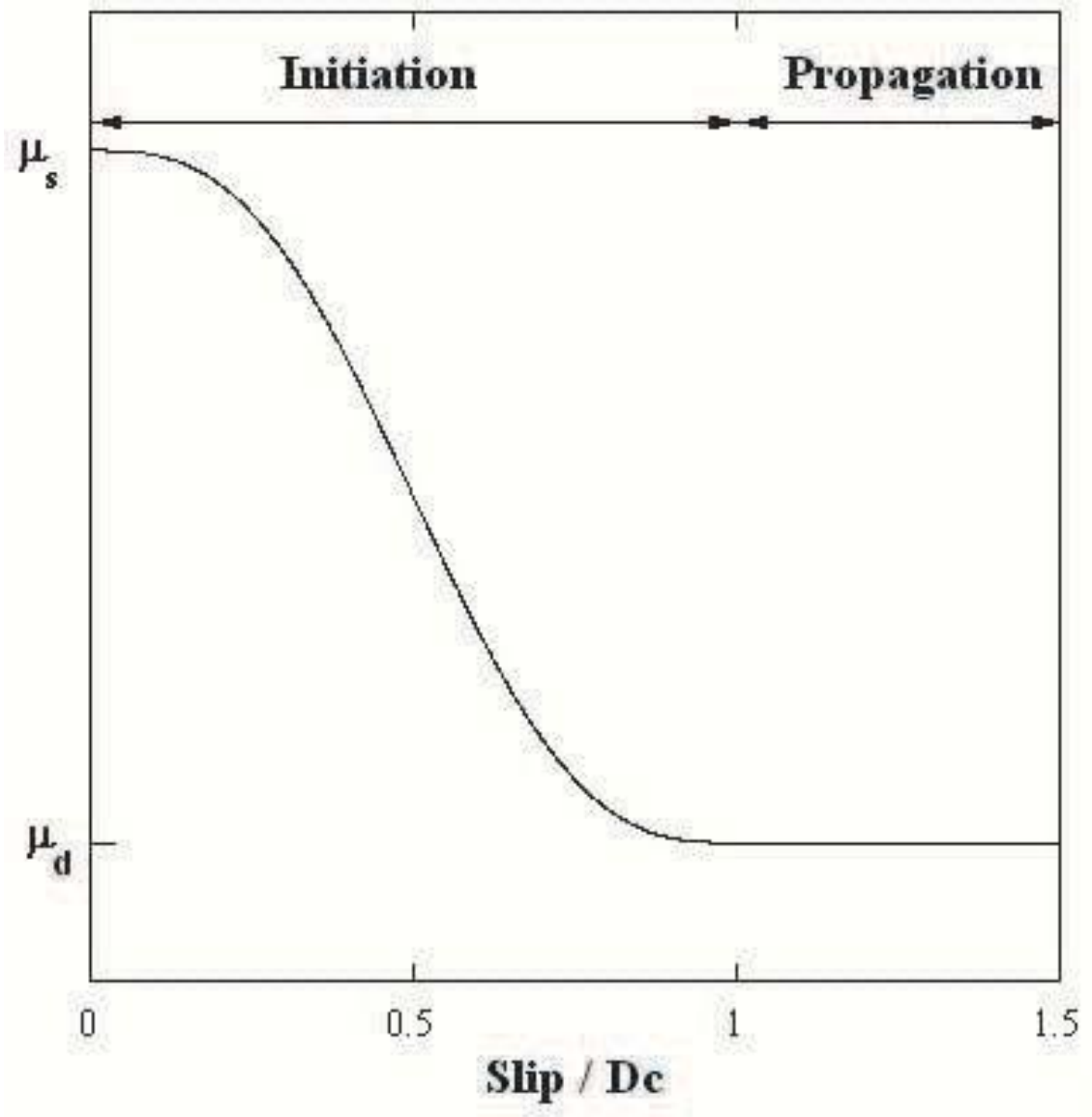

Figure 6:

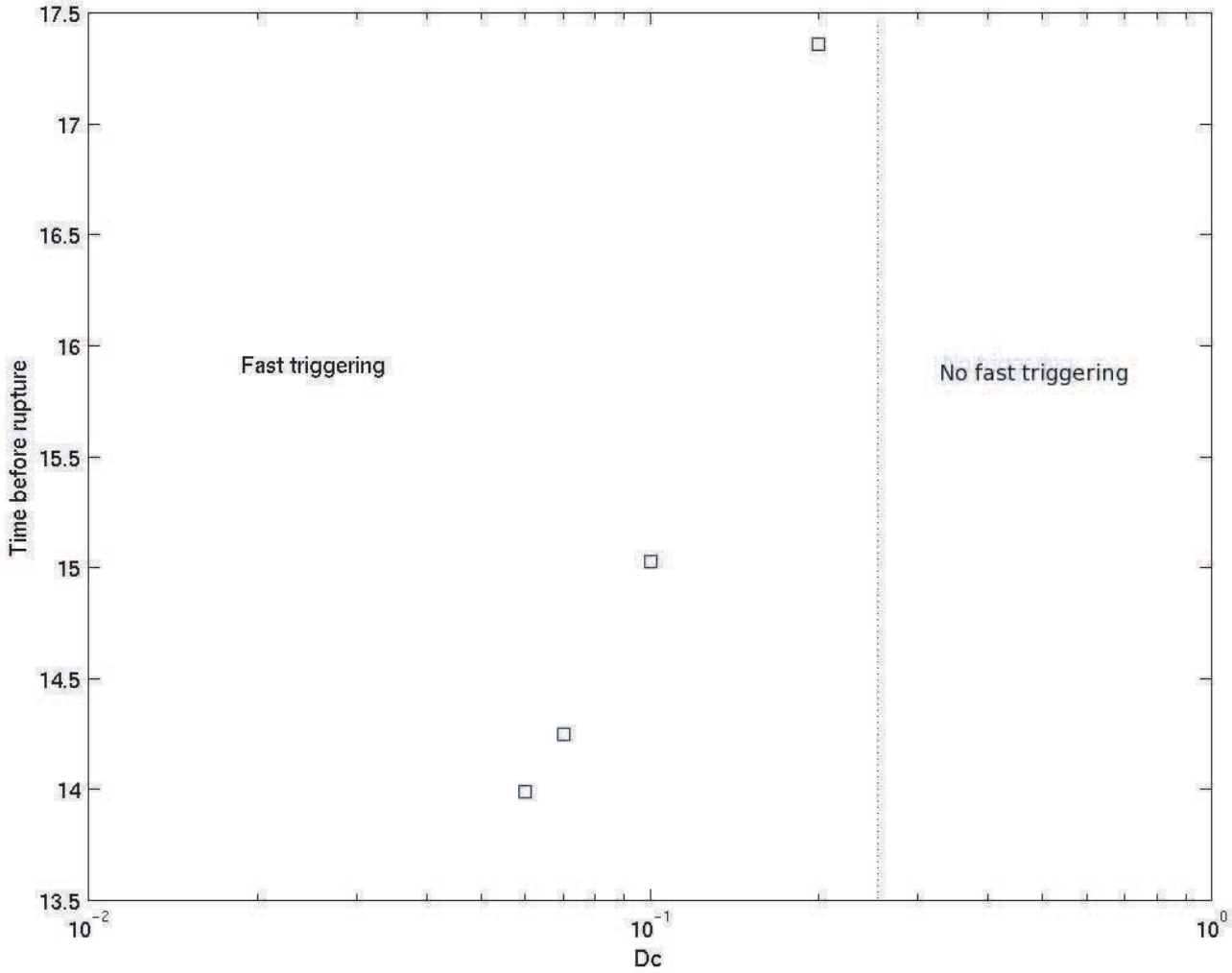
17.5
17
16.5
16
15.5
15
14.5
14
13.5
Time before rupture
Fast triggering
No fast triggering
10^{-2}
10^{-1}
10^{0}
Dc

Figure 7:

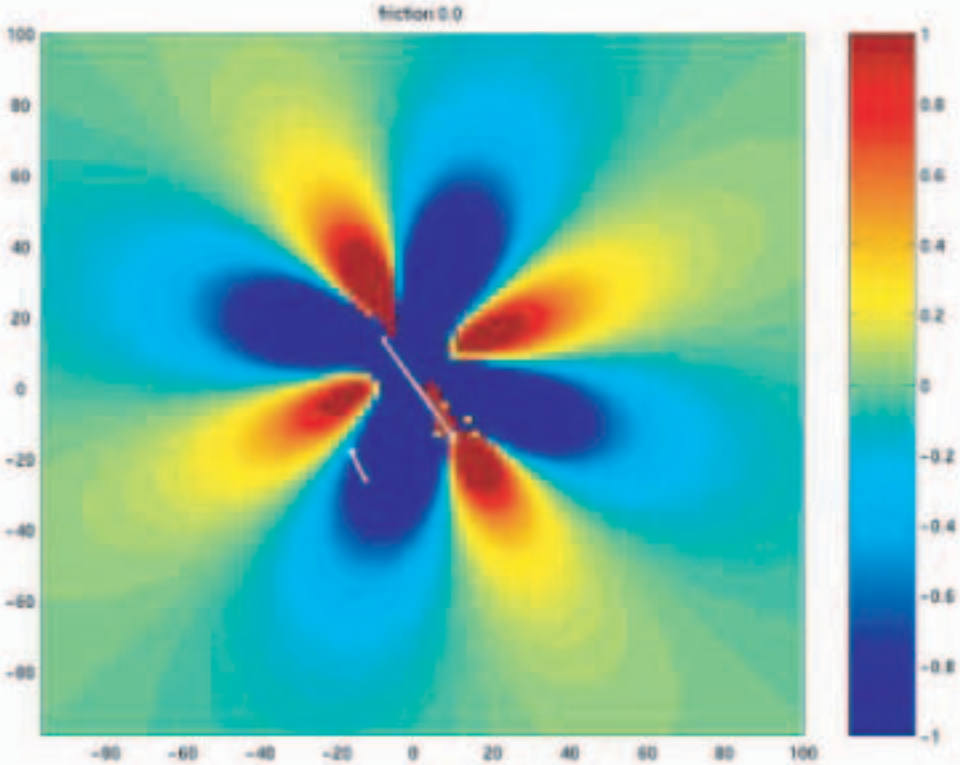
friction 0.0
100
80
60
40
20
0
-20
-40
-60
-80
-80
-60
-40
-20
0
20
40
60
80
100
1
0.8
0.6
0.4
0.2
0
-0.2
-0.4
-0.6
-0.8
-1

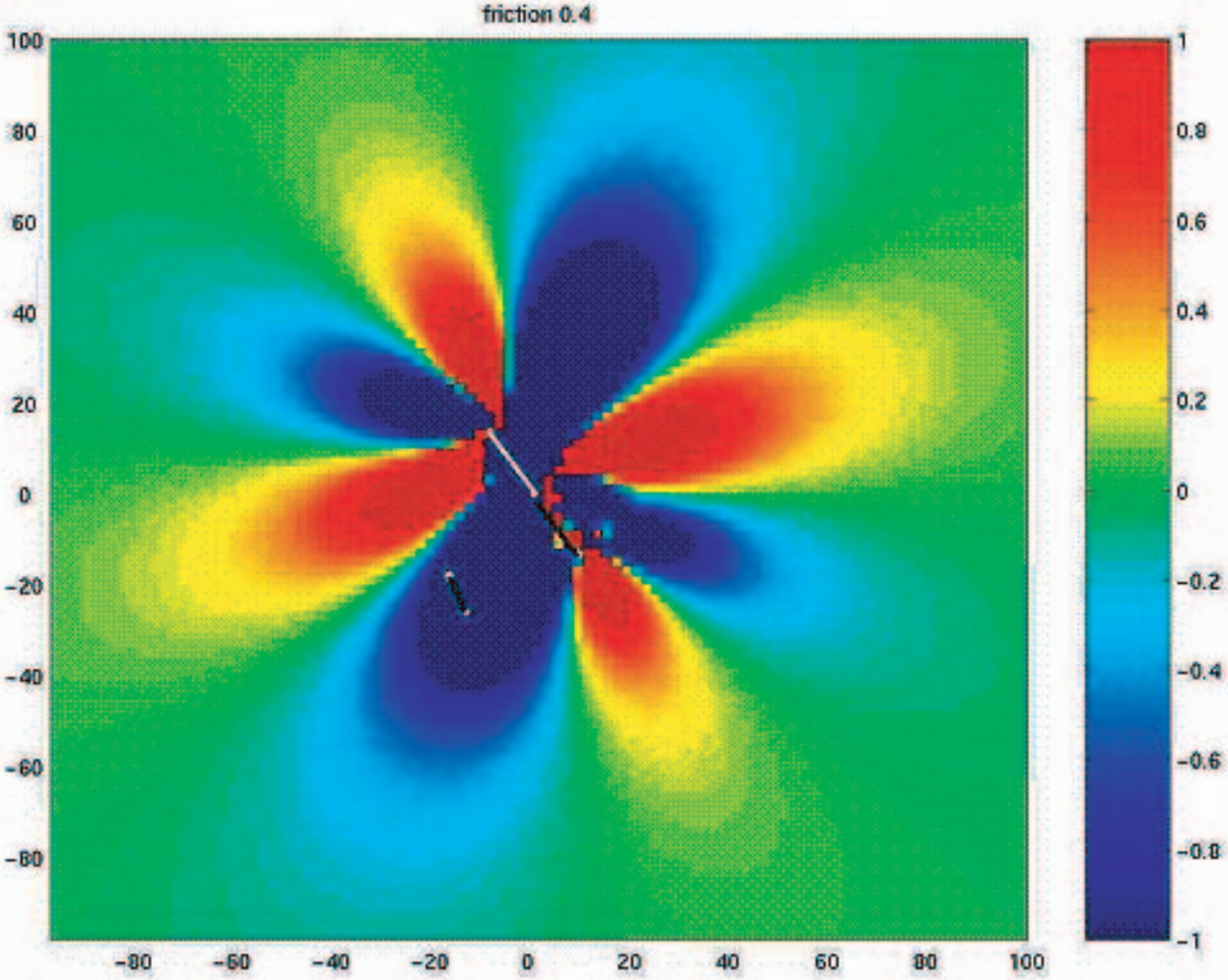
friction 0.4
100
80
60
40
20
0
-20
-40
-60
-80
-80
-60
-40
-20
0
20
40
60
80
100
1
0.8
0.6
0.4
0.2
0
-0.2
-0.4
-0.6
-0.8
-1

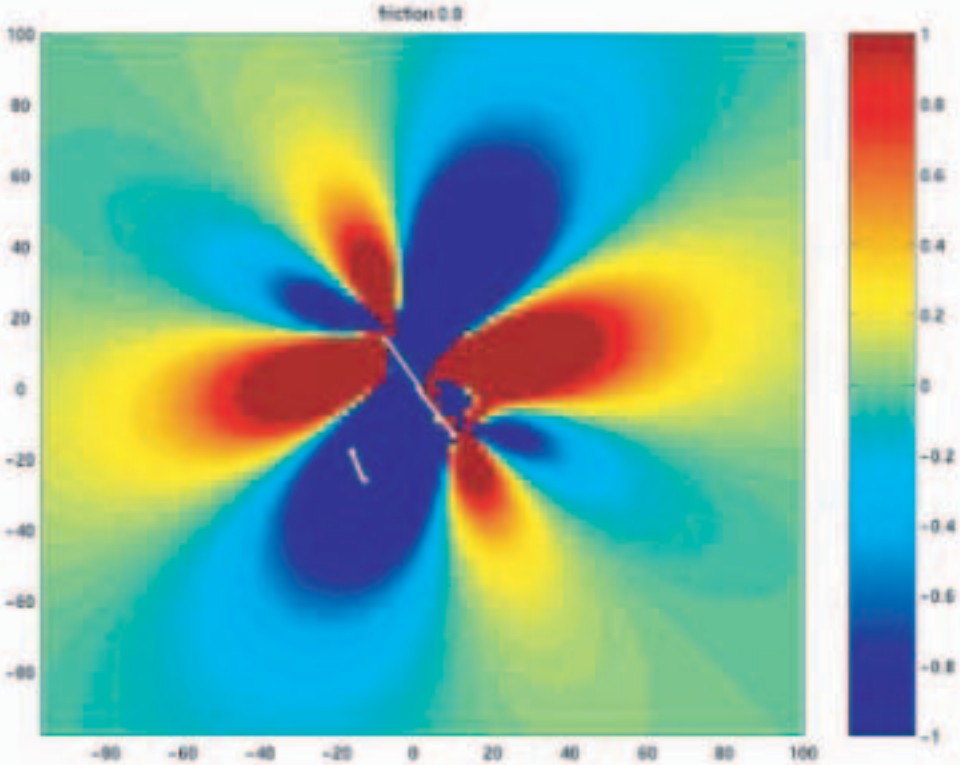
friction 0.0
100
80
60
40
20
0
-20
-40
-60
-80
-80
-60
-40
-20
0
20
40
60
80
100
1
0.8
0.6
0.4
0.2
0
-0.2
-0.4
-0.6
-0.8
-1

Aftershock distribution and virtual station

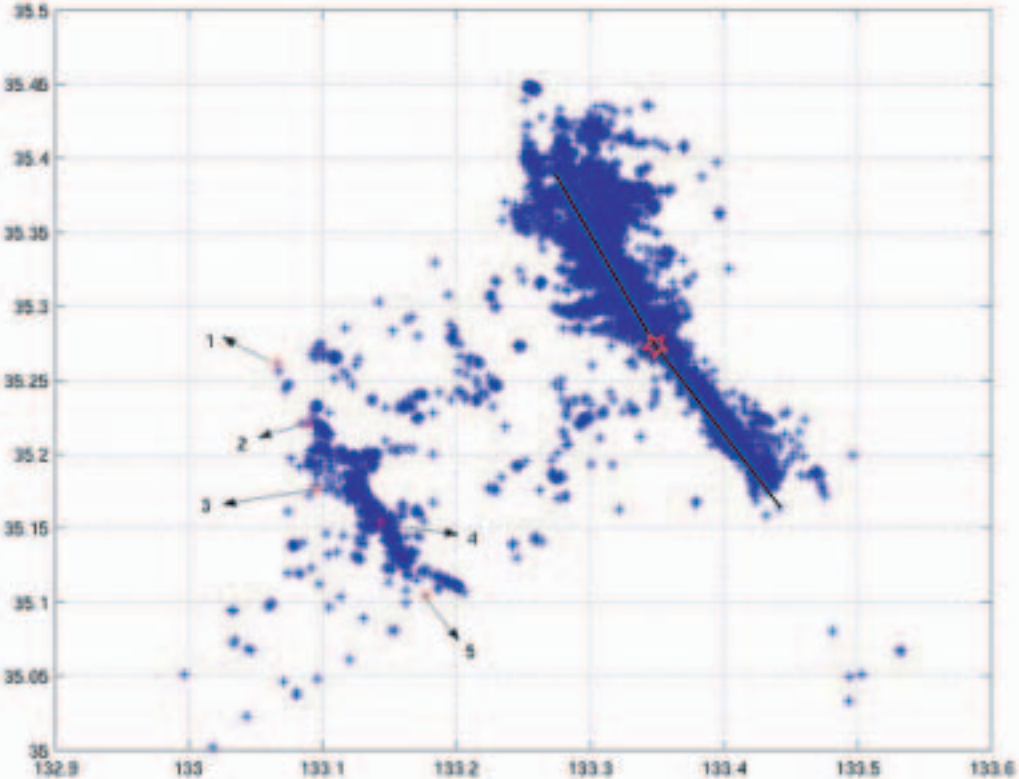

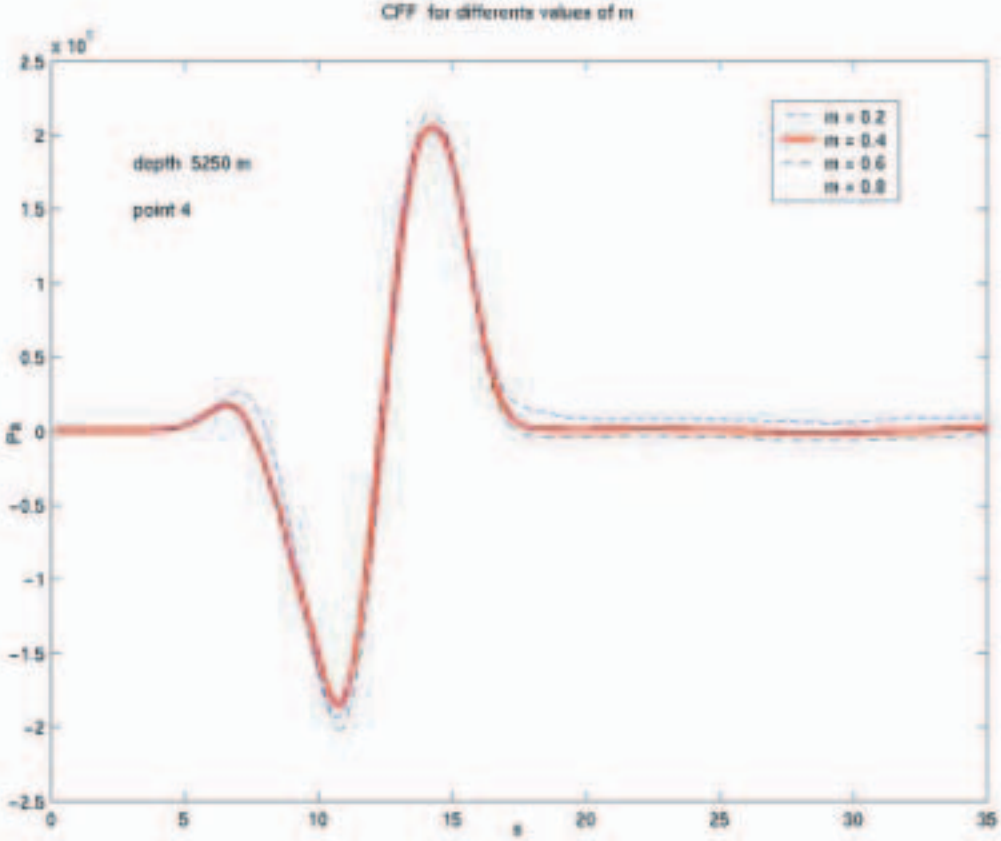
CFF for differents values of m
x 10^7
2.5
2
1.5
1
0.5
0
-0.5
-1
-1.5
-2
-2.5
0
5
10
15
20
25
30
35
s
depth 5250 m
point 4
m = 0.2
m = 0.4
m = 0.6
m = 0.8

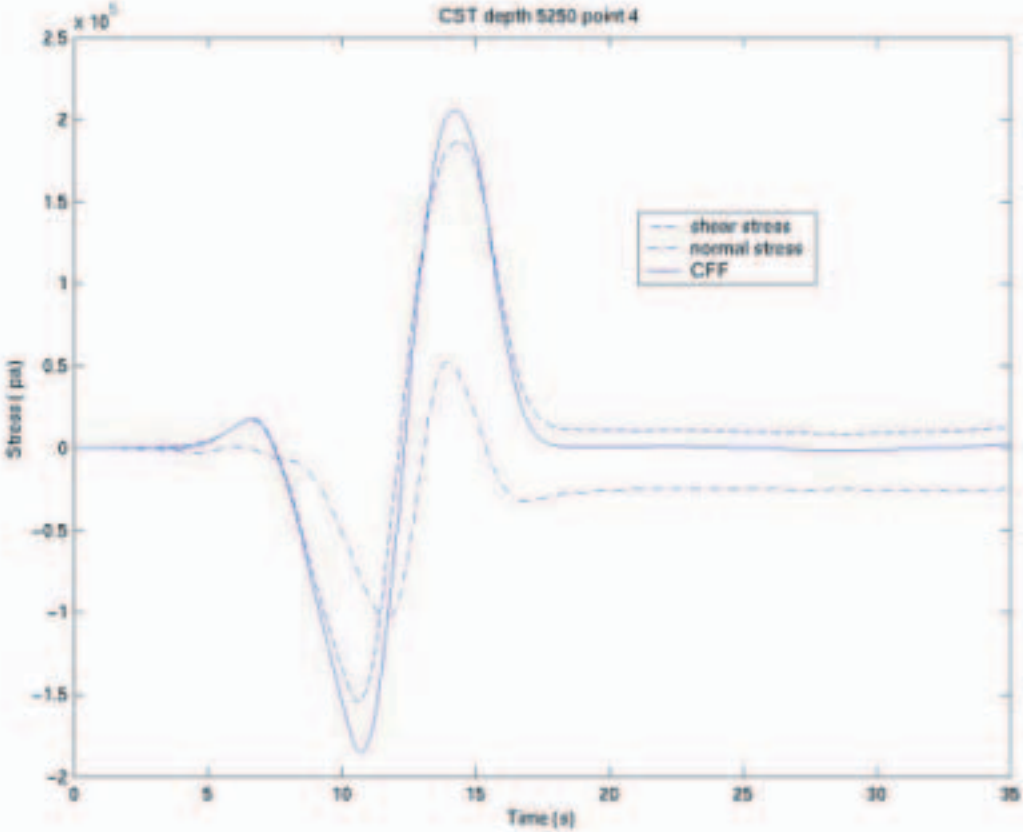
CST depth 5250 point 4
x 10^5
2.5
2
1.5
1
0.5
0
-0.5
-1
-1.5
-2
Stress (psi)
0
5
10
15
20
25
30
35
Time (s)
shear stress
normal stress
CFF

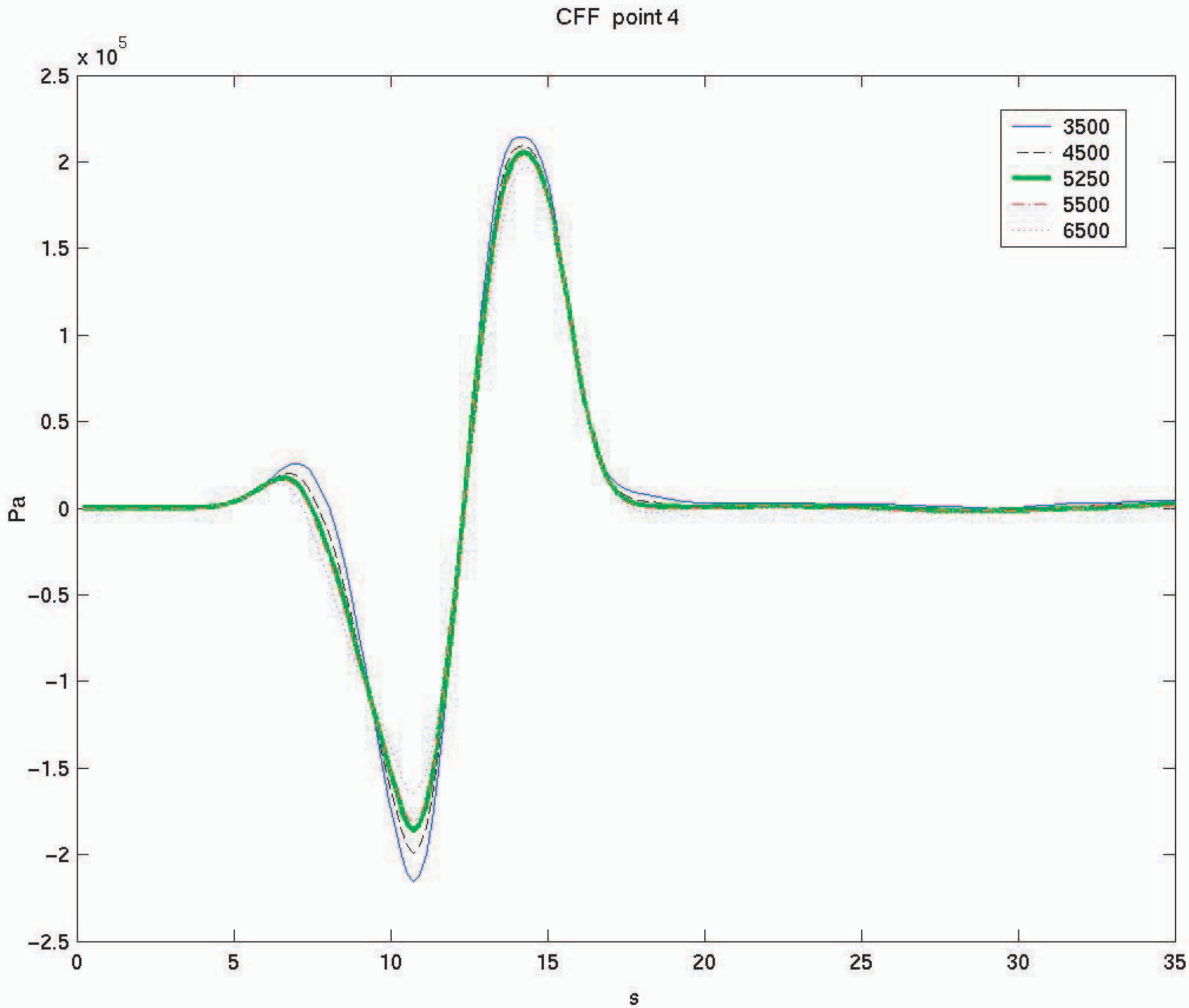
CFF point 4
x 10^5
2.5
2
1.5
1
0.5
0
−0.5
−1
−1.5
−2
−2.5
Pa
0
5
10
15
20
25
30
35
s
3500
4500
5250
5500
6500

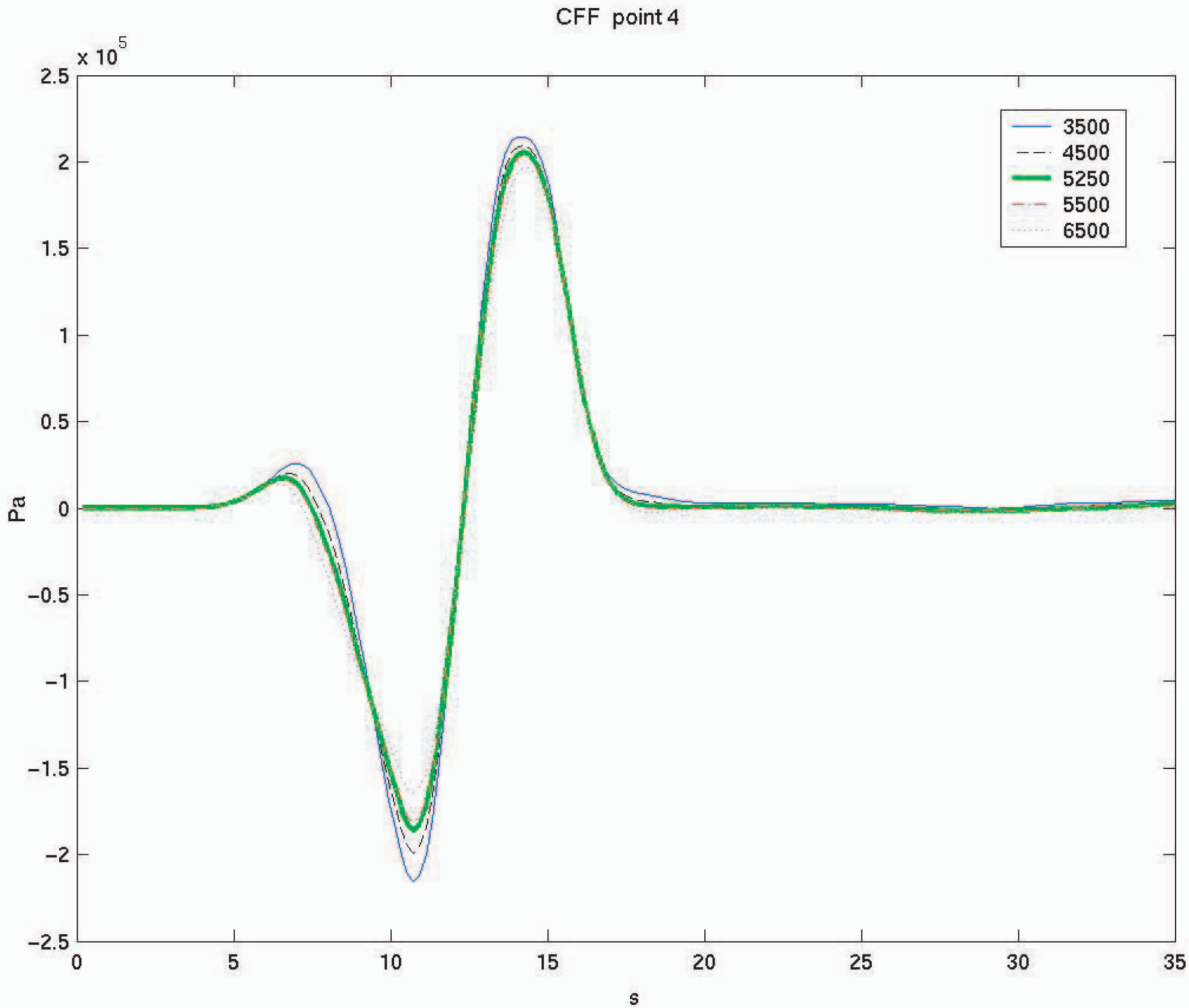
CFF point 4
x 10^5
2.5
2
1.5
1
0.5
0
−0.5
−1
−1.5
−2
−2.5
Pa
0
5
10
15
20
25
30
35
s
3500
4500
5250
5500
6500

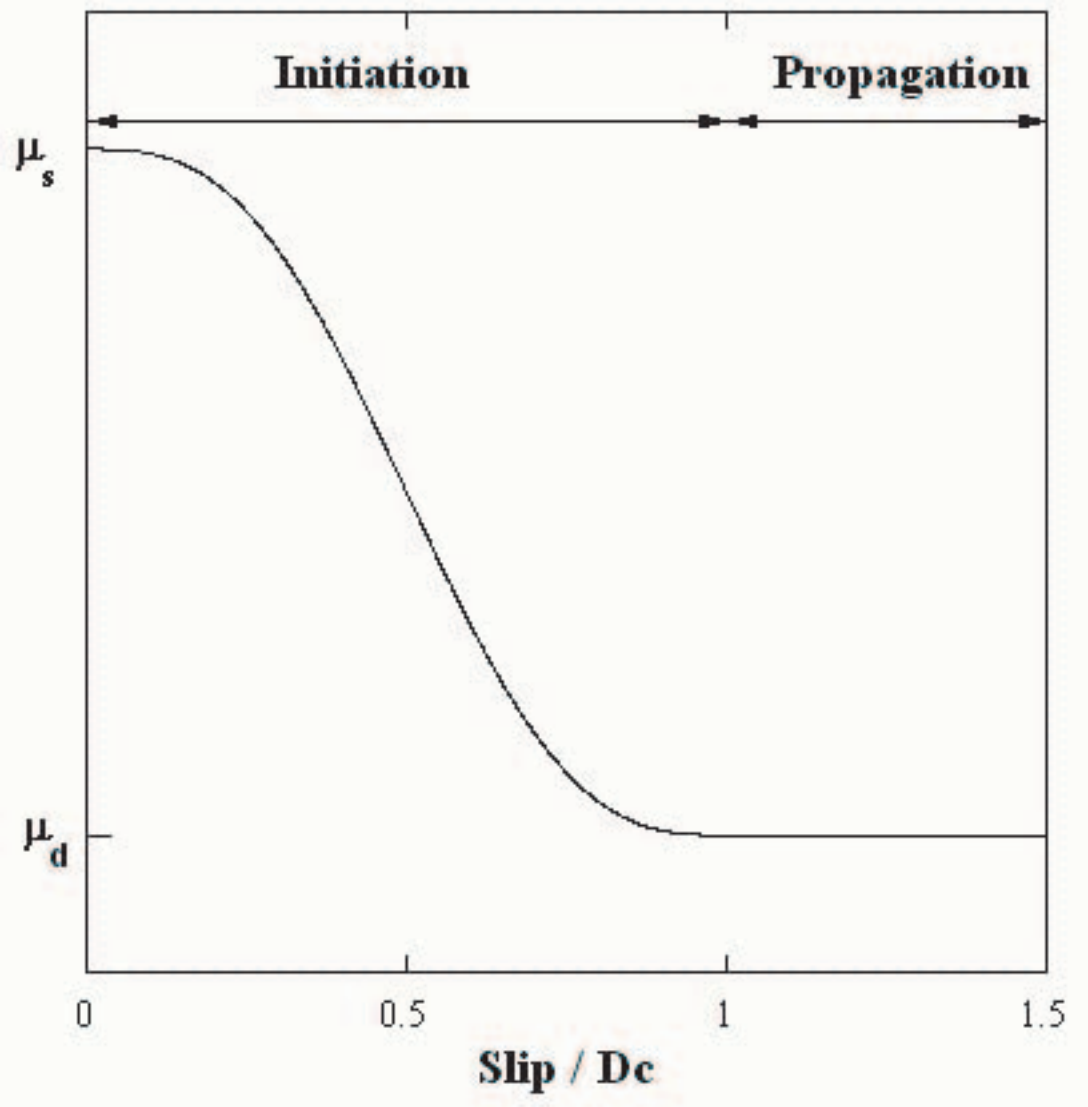
Initiation
Propagation
μs
μd
0
0.5
1
1.5
Slip / Dc

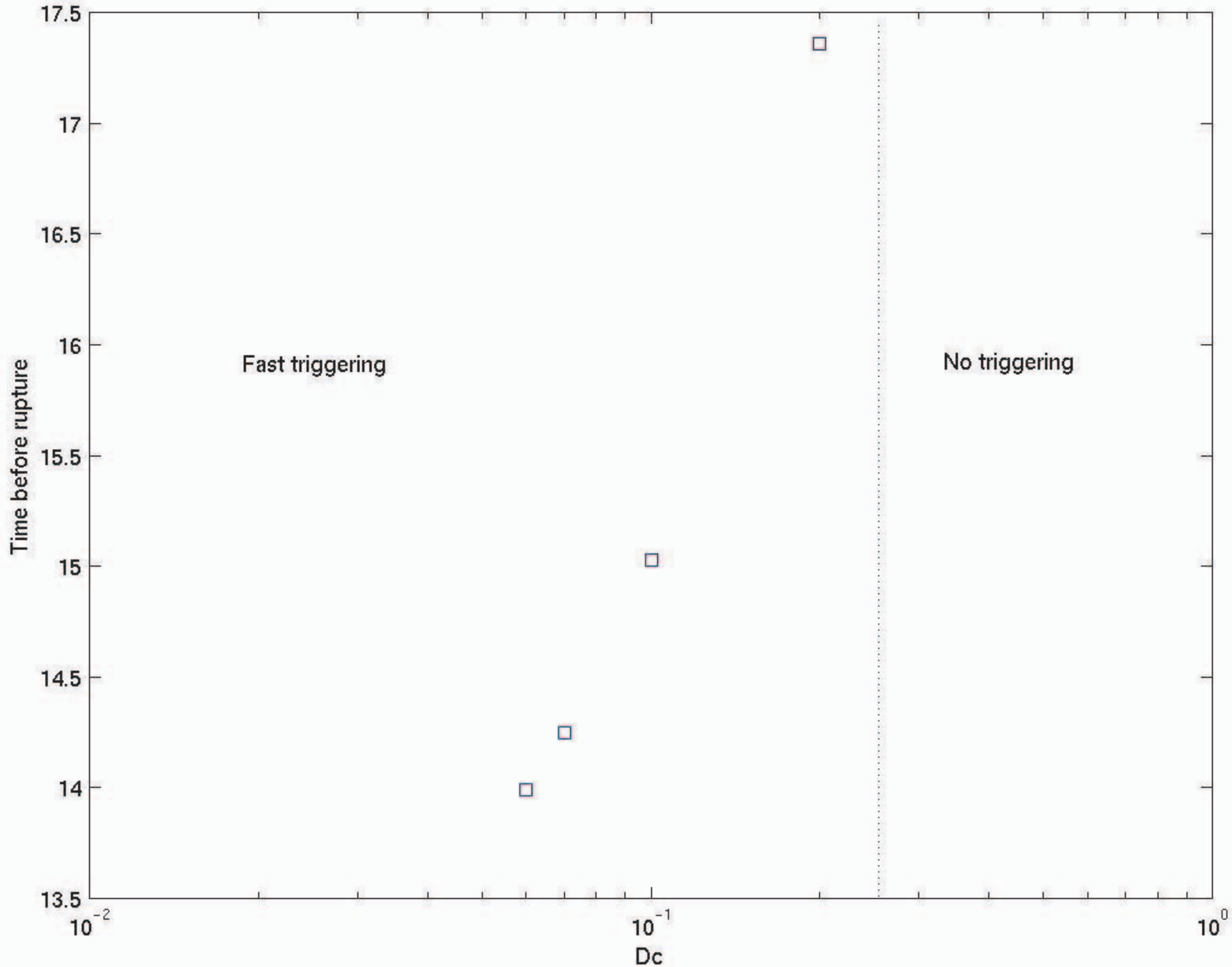
17.5
17
16.5
16
15.5
15
14.5
14
13.5
Time before rupture
Fast triggering
No triggering
10^{-2}
10^{-1}
10^{0}
Dc